PHYSICAL REVIEW D **86,** 124041 (2012)

Space-time diagrammatics

Piotr T. Chruściel[*] and Christa R. Ölz[†]
Gravitational Physics, University of Vienna, Boltzmanngasse 5, A-1090 Vienna, Austria

Sebastian J. Szybka[‡]
Astronomical Observatory, Jagellonian University, Orla 171, 30-244 Kraków, Poland
(Received 22 August 2012; published 20 December 2012)

We introduce a new class of two-dimensional diagrams, the *projection diagrams*, as a tool to visualize the global structure of space-times. We construct the diagrams for several metrics of interest, including the Kerr-Newman-(anti)de Sitter family, with or without cosmological constant, and the Emparan-Reall black rings.

DOI: 10.1103/PhysRevD.86.124041 PACS numbers: 04.20.Jb, 04.20.−q, 97.60.Lf, 04.50.Gh

I. INTRODUCTION

A very useful tool for visualizing the geometry of two-dimensional Lorentzian manifolds is that of *conformal Carter-Penrose diagrams*. Such diagrams have been successfully used to visualize the geometry of two-dimensional sections of the Schwarzschild (cf., e.g., Ref. [1]), Kerr [2,3] and several other [4] geometries. A systematic study of conformal diagrams for time-independent two-dimensional geometries has been carried out in Ref. [5] by Walker; for the convenience of the reader, Walker's analysis is briefly summarized in Sec. II.

For spherically symmetric geometries, the two-dimensional conformal diagrams provide useful information about the four-dimensional geometry as well, since many essential aspects of the space-time geometry are contained in the $t - r$ sector of the metric.

The object of this paper is to show that one can usefully represent classes of nonspherically symmetric geometries in terms of two-dimensional diagrams, which we call *projection diagrams*, using an auxiliary two-dimensional metric, constructed out of the space-time metric. The issues such as stable causality, global hyperbolicity, existence of event or Cauchy horizons, the causal nature of boundaries, and existence of conformally smooth infinities become evident by inspection of the diagrams.

We give a general definition of such diagrams and construct examples for the Kerr-Newman family of metrics, with or without cosmological constant of either sign, and for the Emparan-Reall metrics. We show how the projection diagrams for the Pomeransky-Senkov metrics could be constructed and present a tentative diagram for those metrics. We end the paper by pointing out how the projection diagrams can be used to construct inequivalent extensions of a family of maximal, globally hyperbolic, vacuum or electrovacuum, space-times with compact Cauchy surfaces obtained by periodic identifications of the time coordinate in the Kerr-Newman-(anti)de Sitter family of metrics, as well as for Taub-NUT space-times.

[*]Piotr.Chrusciel@univie.ac.at
[†]a0607354@unet.univie.ac.at
[‡]Sebastian.Szybka@uj.edu.pl

II. CONFORMAL DIAGRAMS FOR STATIC TWO-DIMENSIONAL SPACE-TIMES

Following [5], we construct conformal diagrams for two-dimensional Lorentzian metrics of the form

$$\overset{(2)}{g} = -F(r)dt^2 + F^{-1}(r)dr^2, \tag{1}$$

where F is, for simplicity and definiteness, a real-analytic function on an interval, t ranges over $\mathbb{R}$, and one considers separately maximal intervals in $\mathbb{R}$ on which F is finite and does not change sign; those define the ranges of r. Each such interval leads to a connected Lorentzian manifold on which $\overset{(2)}{g}$ is defined, and the issue is whether or not such manifolds can be patched together, and how. Note that t is *not* a time coordinate in regions where F is negative.

It should be kept in mind that the study of the conformal structure for more general metrics of the form

$$\overset{(2)}{g} = -F(r)H_1(r)dt^2 + F^{-1}(r)H_2(r)dr^2, \tag{2}$$

where H_1 and H_2 are positive in the range of r of interest, can be reduced to the one for the metric (1) by writing

$$\overset{(2)}{g} = \sqrt{H_1H_2}(-\hat{F}dt^2 + \hat{F}^{-1}dr^2), \tag{3}$$

where $\hat{F} = \sqrt{\frac{H_1}{H_2}}F$.

A. Manifest conformal flatness

In order to bring the metric (1) to a manifestly conformally flat form, one chooses a value of r_* such that $F(r_*) \neq 0$ and introduces a new coordinate x defined as

$$x(r) = \int_{r_*}^{r} \frac{ds}{F(s)} \Rightarrow dx = \frac{dr}{F(r)}, \tag{4}$$

leading to

$$\overset{(2)}{g} = -F dt^2 + \frac{1}{F}(F dx)^2 = F(-dt^2 + dx^2). \tag{5}$$

The geometry of the space-time, and its possible extendability, will depend upon the sign of F, the zeros of F, and their order. For example, whenever x ranges over $\mathbb{R}$ the space-time $(\mathbb{R}^2, \overset{(2)}{g})$ can be conformally mapped to the following *diamond*:

$$\{-\pi/2 < T - X < \pi/2, -\pi/2 < T + X < \pi/2\} \subset \mathbb{R}^2.$$

This is done by first introducing

$$u = t - x, \quad v = t + x \Longleftrightarrow t = \frac{u+v}{2}, \quad x = \frac{v-u}{2}, \tag{6}$$

which brings $\overset{(2)}{g}$ into the form

$$\overset{(2)}{g} = -du dv.$$

While some other ranges of variables might arise in specific examples, in the current case we have $(u, v) \in \mathbb{R}^2$. We bring the last $\mathbb{R}^2$ to a bounded set using

$$U = \arctan(u), \qquad V = \arctan(v), \tag{7}$$

and thus

$$(U, V) \in \left(-\frac{\pi}{2}, \frac{\pi}{2}\right) \times \left(-\frac{\pi}{2}, \frac{\pi}{2}\right).$$

This looks somewhat more familiar if we make one last change of coordinates similar to that in (6):

$$U = T - X, \quad V = T + X \Longleftrightarrow T = \frac{U+V}{2}, \quad X = \frac{V-U}{2}, \tag{8}$$

see Fig. 1, leading to

$$\overset{(2)}{g} = \frac{1}{\cos^2(T-X)\cos^2(T+X)}(-dT^2 + dX^2).$$

Simple variations of the above coordinate transformations might be used for alternative ranges of x. An integral of $1/F$ which is infinite near one of the integration bounds and finite at the other one leads to triangles, obtained by cutting a diamond across a diagonal; the sign of F determines which diagonal is relevant. A finite integral of $1/F$ leads to strips, if one does not perform the subsequent coordinate transformation (7). These are then the building blocks, out of which the final maximal diagrams can be built.

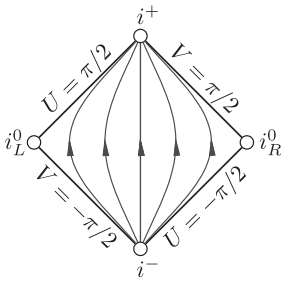

FIG. 1. The conformal diagram for (1 + 1)-dimensional Minkowski space-time.

B. Gluing

We pass now to the gluing question. It turns out that *four blocks* can be glued together across a boundary $\{r = r_0\}$ at which

$$F(r_0) = 0, \qquad F'(r_0) \neq 0.$$

Since F has a simple zero, it factorizes as

$$F(r) = (r - r_0)H(r),$$

for a function H which has no zeros in a neighborhood of r_0. The gluing is done in two steps by defining

$$\begin{aligned} &u = t - f(r), \qquad v = t + f(r), \qquad f' = \frac{1}{F}, \\ &\hat{u} = -\exp(-cu), \qquad \hat{v} = \exp(cv), \end{aligned} \tag{9}$$

where

$$c = \frac{F'(r_0)}{2}.$$

This leads to the following form of the metric:

$$\overset{(2)}{g} = \mp \frac{4H(r)}{(F'(r_0))^2} \exp(-\hat{f}(r)F'(r_0)) d\hat{u} d\hat{v}, \tag{10}$$

with a negative sign if we started in the region $r > r_0$ and positive otherwise. Here

$$\hat{f}(r) := f(r) - \frac{1}{F'(r_0)} \ln|r - r_0|.$$

In (10) the function r should be viewed as a function of the product $\hat{u}\,\hat{v}$, implicitly defined by the equation

$$\hat{u}\,\hat{v} = \mp(r - r_0)\exp(\hat{f}(r)F'(r_0)).$$

Note that for analytic F's the extension so constructed is real analytic; this follows from the analytic version of the implicit function theorem.

Boundaries at finite distance $r = r_0$ but at which F has a zero of higher order can still be glued together via *two-block gluing*. Here one continues to use the functions u and v defined in (9), but now one does *not* use u and v simultaneously as coordinates. Instead one considers a coordinate system (u, r), so that

$$\overset{(2)}{g} = -F\left(du + \frac{1}{F}dr\right)^2 + \frac{1}{F}dr^2 = -F du^2 - 2 du dr.$$

Since $\det \overset{(2)}{g} = -1$, the resulting metric extends smoothly as a Lorentzian metric to the whole nearby interval where F is defined. This will certainly include the nearest

conformal block, as well as some further ones if the case arises. A distinct extension is obtained when using instead the coordinate system (v, r).

Asymptotic regions where $|r| \to \infty$ but F is bounded, and bounded away from zero, provide null conformal boundaries at infinity.

III. PROJECTION DIAGRAMS

A. The definition

Let $(\mathcal{M}, g)$ be a smooth space-time, and let $\mathbb{R}^{1,n}$ denote the $(n+1)$-dimensional Minkowski space-time. A *projection diagram* is a pair $(\pi, \mathcal{U})$, where

$$\pi: \mathcal{M} \to \mathcal{W}$$

is a continuous map, differentiable on an open dense set, from $\mathcal{M}$ onto $\pi(\mathcal{M}) =: \mathcal{W} \subset \mathbb{R}^{1,1}$, together with an open set

$$\mathcal{U} \subset \mathcal{M},$$

assumed to be nonempty, on which π is a smooth submersion, so that it holds:

(1) every smooth timelike curve $\sigma \subset \pi(\mathcal{U})$ is the projection of a smooth timelike curve γ in $(\mathcal{U}, g)$: $\sigma = \pi \circ \gamma$;

(2) the image $\pi \circ \gamma$ of every smooth timelike curve $\gamma \subset \mathcal{U}$ is a timelike curve in $\mathbb{R}^{1,1}$.

Some comments are in order.

First, we have assumed for simplicity that $(\mathcal{M}, g)$, $\pi|_{\mathcal{U}}$, and the causal curves in the definition are smooth, though this is unnecessary for most purposes.

Next, we do not assume that π is a submersion, or in fact differentiable, everywhere on $\mathcal{M}$. This allows us to talk about "the projection diagram of Minkowski space-time," or "the projection diagram of Kerr space-time," rather than of "the projection diagram of the subset $\mathcal{U}$ of Minkowski space-time," etc. Note that the latter terminology would be more precise, and will sometimes be used, but appears to be an overkill in most cases.

Further, the requirement that timelike curves in $\pi(\mathcal{U})$ arise as projections of timelike curves in $\mathcal{M}$ ensures that causal relations on $\pi(\mathcal{U})$, which can be seen by inspection of $\pi(\mathcal{U})$, reflect causal relations on $\mathcal{M}$. Conditions 1 and 2 taken together ensure that causality on $\pi(\mathcal{U})$ represents as accurately as possible causality on $\mathcal{U}$.

By continuity, images of causal curves in $\mathcal{U}$ are causal in $\pi(\mathcal{U})$. Note that null curves in $\mathcal{U}$ are often mapped to timelike ones in $\pi(\mathcal{U})$.

The second condition of the definition is of course equivalent to the requirement that the images by π_* of timelike vectors in $T\mathcal{U}$ are timelike. This implies further that the images by π_* of causal vectors in $T\mathcal{U}$ are causal. One should keep in mind that images by π_* of null vectors in $T\mathcal{U}$ could be timelike. And, of course, many spacelike vectors will be mapped to causal vectors under π_*.

Recall that π is a submersion if π_* is surjective at every point. The requirement that π is a submersion guarantees that open sets are mapped to open sets. This, in turn, ensures that projection diagrams with the same set $\mathcal{U}$ are locally unique, up to a local conformal isometry of two-dimensional Minkowski space-time. We do not know whether or not two surjective projection diagrams π_i: $\mathcal{U} \to \mathcal{W}_i$, $i = 1, 2$, with identical domain of definition $\mathcal{U}$ are globally unique, up to a conformal isometry of $\mathcal{W}_1$ and $\mathcal{W}_2$. It would be of interest to settle this question.

In many examples of interest the set $\mathcal{U}$ will *not* be connected.

Note that a necessary condition for existence of a projection diagram is *stable causality* of $\mathcal{U}$: indeed, let t be any time function on $\mathbb{R}^{1,1}$, then $t \circ \pi$ is a time function on $\mathcal{U}$.

It might be tempting to require that $\mathcal{U}$ be dense in $\mathcal{M}$. Such a requirement would, however, prohibit one to construct a projection diagram of the usual maximal extension of Kerr space-time, since the latter contains open regions which are not stably causal.

Recall that a map is proper if inverse images of compact sets are compact. One could further require π to be proper; indeed, many projection diagrams below have this property. This is actually useful, as then the inverse images of globally hyperbolic subsets of $\mathcal{W}$ are globally hyperbolic, and so global hyperbolicity, or lack thereof, can be established by visual inspection of $\mathcal{W}$. It appears, however, more convenient to talk about *proper projection diagrams* whenever π is proper, allowing for nonproperness in general.

As such, we have assumed for simplicity that π maps $\mathcal{M}$ into a subset of Minkowski space-time. In some applications it might be natural to consider more general two-dimensional manifolds as the target of π; this requires only a trivial modification of the definition. An example is provided by the Gowdy metrics on a torus, discussed at the end of this section, where the natural image manifold for π is $(-\infty, 0) \times S^1$, equipped with a flat product metric. Similarly, maximal extensions of the class of Kerr-Newman-de Sitter metrics of Fig. 8 require the image of π to be a suitable Riemann surface.

B. Simplest examples

The simplest examples of projection diagrams can be constructed for metrics of the form

$$g = e^f(-F dt^2 + F^{-1} dr^2) + \underbrace{h_{AB} dx^A dx^B}_{=:h}, \qquad (11)$$

with $F = F(r)$, where $h = h_{AB}(t, r, x^C) dx^A dx^B$ is a family of *Riemannian* metrics on an $(n-1)$-dimensional manifold N^{n-1}, possibly depending upon t and r, and f is a function which is allowed to depend upon all variables. It should be clear that any manifestly conformally flat representation of any extension, defined on $\mathcal{W} \subset \mathbb{R}^{1,1}$, of the

two-dimensional metric $-Fdt^2 + F^{-1}dr^2$, as discussed in Sec. II, provides immediately a projection diagram for $(\mathcal{W} \times N^{n-1}, g)$.

In particular, introducing spherical coordinates (t, r, x^A) on

$$\mathcal{U} := \{(t, \vec{x}) \in \mathbb{R}^{n+1}, |\vec{x}| \neq 0\} \subset \mathbb{R}^{1,n} \tag{12}$$

and forgetting about the $(n-1)$-sphere part of the metric leads to a projection diagram for Minkowski space-time which coincides with the usual conformal diagram of the fixed-angles subsets of Minkowski space-time (see the left figure in Fig. 14 below; the shaded region there should be left unshaded in the Minkowski case). The set $\mathcal{U}$ defined in (12) cannot be extended to include the world line passing through the origin of $\mathbb{R}^n$ since the map π fails to be differentiable there. This diagram is proper but fails to represent correctly the nature of the space-time near the set $|\vec{x}| = 0$.

On the other hand, a globally defined projection diagram for Minkowski space-time [thus, $(\mathcal{U}, g) = \mathbb{R}^{1,n}$] can be obtained by writing $\mathbb{R}^{1,n}$ as a product $\mathbb{R}^{1,1} \times \mathbb{R}^{n-1}$ and forgetting about the second factor. This leads to a projection diagram of Fig. 1. This diagram, which is not proper, fails to represent correctly the connectedness of $\mathcal{I}^+$ and $\mathcal{I}^-$ when $n > 1$.

It will be seen in Sec. III H that yet another choice of π and of the set $(\mathcal{U}, g) \subset \mathbb{R}^{1,n}$ leads to a third projection diagram for Minkowski space-time.

A further example of nonuniqueness is provided by the projection diagrams for Taub-NUT metrics, discussed in Sec. IV B.

These examples show that there is no uniqueness in the projection diagrams and that various such diagrams might carry different information about the causal structure. It is clear that for space-times with intricate causal structure, some information will be lost when projecting to two dimensions. This raises the interesting question, whether there exists a notion of optimal projection diagram for specific space-times. In any case, the examples we give in what follows appear to depict the essential causal properties of the associated space-time, except perhaps for the black ring diagrams of Secs. III H and III I.

Nontrivial examples of metrics of the form (11) are provided by the Gowdy metrics on a torus [6], which can be written in the form [6,7]

$$\begin{aligned} g = {} & e^f(-dt^2 + d\theta^2) \\ & + |t|(e^P(dx^1 + Qdx^2)^2 + e^{-P}(dx^2)^2), \end{aligned} \tag{13}$$

with $t \in (-\infty, 0)$ and $(\theta, x^1, x^2) \in S^1 \times S^1 \times S^1$. Unwrapping θ from S^1 to $\mathbb{R}$ and projecting away the dx^1 and dx^2 factors, one obtains a projection diagram the image of which is the half-space $t < 0$ in Minkowski space-time. This can be further compactified as in Sec. II A, keeping in mind that the asymptotic behavior of the metric for large negative values of t [8] is not compatible with the existence of a smooth conformal completion of the full space-time metric across past null infinity. Note that this projection diagram fails to represent properly the existence of Cauchy horizons for nongeneric [9] Gowdy metrics.

Similarly, generic Gowdy metrics on $S^1 \times S^2$, S^3, or $L(p, q)$ can be written in the form [6,7]

$$\begin{aligned} g = {} & e^f(-dt^2 + d\theta^2) + R_0 \sin(t)\sin(\theta) \times (e^P(dx^1 \\ & + Qdx^2)^2 + e^{-P}(dx^2)^2), \end{aligned} \tag{14}$$

with $(t, \theta) \in (0, \pi) \times [0, \pi]$, leading to the Gowdy square as the projection diagram for the space-time. [This is the diagram of Fig. 13, where the lower boundary corresponds to $t = 0$, the upper boundary corresponds to $t = \pi$, the left boundary corresponds to the axis of rotation $\theta = 0$, and the right boundary is the projection of the axis of rotation $\theta = \pi$. The diagonals, denoted as $y = y_h$ in Fig. 13, correspond in the Gowdy case to the projection of the set where the gradient of the area $R = R_0 \sin(t)\sin(\theta)$ of the orbits of the isometry group $\mathrm{U}(1) \times \mathrm{U}(1)$ vanishes, and do not have any further geometric significance. The lines with the arrows in Fig. 13 are irrelevant for the Gowdy metrics, as the orbits of the isometry group of the space-time metric are spacelike throughout the Gowdy square.]

In the remainder of this work we will construct projection diagrams for families of metrics of interest which are not of the simple form (11).

C. The Kerr metrics

Consider the Kerr metric in Boyer-Lindquist coordinates,

$$\begin{aligned} g = {} & -\frac{\Delta_r - a^2\sin^2(\theta)}{\Sigma}dt^2 + \frac{\Sigma}{\Delta_r}dr^2 + \Sigma d\theta^2 \\ & + \frac{\sin^2(\theta)((r^2 + a^2)^2 - a^2\sin^2(\theta)\Delta_r)}{\Sigma}d\varphi^2 \\ & - \frac{2a\sin^2(\theta)(r^2 + a^2 - \Delta_r)}{\Sigma}dtd\varphi. \end{aligned} \tag{15}$$

Here

$$\begin{aligned} \Sigma &= r^2 + a^2\cos^2\theta, \\ \Delta_r &= r^2 + a^2 - 2mr = (r - r_+)(r - r_-), \end{aligned} \tag{16}$$

for some real parameters a and m, with

$$r_\pm = m \pm (m^2 - a^2)^{\frac{1}{2}},$$

and we assume that $0 < |a| \leq m$. We note that

$$\begin{aligned} g_{\varphi\varphi} &= \sin^2(\theta)\left(\frac{2a^2mr\sin^2(\theta)}{a^2\cos^2(\theta) + r^2} + a^2 + r^2\right) \\ &= \frac{\sin^2(\theta)(a^4 + a^2\cos(2\theta)\Delta_r + a^2r(2m + 3r) + 2r^4)}{a^2\cos(2\theta) + a^2 + 2r^2}, \end{aligned} \tag{17}$$

the first line making clear the non-negativity of $g_{\varphi\varphi}$ for $r \geq 0$.

In the region where ∂_φ is spacelike we rewrite the $t-\varphi$ part of the metric as

$$g_{tt}dt^2 + 2g_{t\varphi}dtd\varphi + g_{\varphi\varphi}d\varphi^2 = g_{\varphi\varphi}\left(d\varphi + \frac{g_{t\varphi}}{g_{\varphi\varphi}}dt\right)^2 + \left(g_{tt} - \frac{g_{t\varphi}^2}{g_{\varphi\varphi}}\right)dt^2, \quad (18)$$

with

$$g_{tt} - \frac{g_{t\varphi}^2}{g_{\varphi\varphi}} = -\frac{2\Delta_r\Sigma}{a^4 + a^2\Delta_r\cos(2\theta) + a^2r(2m+3r) + 2r^4}.$$

For $r > 0$ and $\Delta_r > 0$ it holds that

$$\frac{\Delta_r\Sigma}{(a^2+r^2)^2} \leq \left| g_{tt} - \frac{g_{t\varphi}^2}{g_{\varphi\varphi}} \right| \leq \frac{\Delta_r\Sigma}{r(a^2(2m+r)+r^3)}, \quad (19)$$

with the infimum attained at $\theta \in \{0, \pi\}$ and maximum at $\theta = \pi/2$.

In the region $r > 0$, $\Delta_r > 0$ consider any vector

$$X = X^t\partial_t + X^r\partial_r + X^\theta\partial_\theta + X^\varphi\partial_\varphi,$$

which is causal for the metric g. Let $\Omega(r, \theta)$ be any positive function. Since both $g_{\theta\theta}$ and the first term in (18) are positive, while the coefficient of dt^2 in (18) is negative, we have

$$\begin{aligned} 0 &\geq \Omega^2 g(X,X) = \Omega^2 g_{\mu\nu}X^\mu X^\nu \\ &\geq \Omega^2\left(g_{tt} - \frac{g_{t\varphi}^2}{g_{\varphi\varphi}}\right)(X^t)^2 + \Omega^2 g_{rr}(X^r)^2 \\ &\geq -\sup_\theta\left(\Omega^2\left|g_{tt} - \frac{g_{t\varphi}^2}{g_{\varphi\varphi}}\right|\right)(X^t)^2 + \inf_\theta(\Omega^2 g_{rr})(X^r)^2. \end{aligned} \quad (20)$$

To guarantee the requirements of the definition of a projection diagram, it is simplest to choose Ω so that both extrema in (20) are attained at the same value of θ, say θ_*, while keeping those features of the coefficients which are essential for the problem at hand. It is convenient, but not essential, to have θ_* independent of r. We will make the choice

$$\Omega^2 = \frac{r^2 + a^2}{\Sigma}, \quad (21)$$

but other choices are possible and might be more convenient for other purposes. [The Σ factor has been included to get rid of the angular dependence in $\Omega^2 g_{rr}$, while the numerator has been added to ensure that the metric coefficient γ_{rr} in (23) tends to one as r recedes to infinity, reflecting the asymptotic behavior for large r of the corresponding function $\hat{F}$ in (3).] With this choice of Ω, (20) is equivalent to the statement that

$$\pi_*(X) := X^t\partial_t + X^r\partial_r \quad (22)$$

is a causal vector in the two-dimensional Lorentzian metric

$$\gamma := -\frac{\Delta_r(r^2+a^2)}{r(a^2(2m+r)+r^3)}dt^2 + \frac{(r^2+a^2)}{\Delta_r}dr^2. \quad (23)$$

Using the methods of Walker [5], as reviewed in Sec. II, in the region $r_+ < r < \infty$, the metric γ is conformal to a flat metric on the interior of a diamond, with the conformal factor extending smoothly across that part of its boundary at which $r \to r_+$ when $|a| < m$. This remains true when $|a| = m$ except at the leftmost corner i_L^0 of Fig. 1.

To avoid ambiguities, at this stage π is the projection map $(t, r, \theta, \varphi) \mapsto (t, r)$. The fact that g-causal curves are mapped to γ-causal curves follows from the construction of γ. In order to prove the lifting property, let $\sigma(s) = (t(s), r(s))$ be a γ-causal curve, and then the curve

$$(t(s), r(s), \pi/2, \varphi(s)),$$

where $\varphi(s)$ satisfies

$$\frac{d\varphi}{ds} = -\frac{g_{t\varphi}}{g_{\varphi\varphi}}\frac{dt}{ds},$$

is a g-causal curve which projects to σ.

For causal vectors in the region $r > 0$, $\Delta_r < 0$, we have instead

$$\begin{aligned} 0 &\geq \Omega^2 g(X,X) \geq \Omega^2\left(g_{tt} - \frac{g_{t\varphi}^2}{g_{\varphi\varphi}}\right)(X^t)^2 + \Omega^2 g_{rr}(X^r)^2 \\ &\geq \inf_\theta\left(\Omega^2\left|g_{tt} - \frac{g_{t\varphi}^2}{g_{\varphi\varphi}}\right|\right)(X^t)^2 - \sup_\theta(\Omega^2|g_{rr}|)(X^r)^2. \end{aligned} \quad (24)$$

Since the inequalities in (19) are reversed when $\Delta_r < 0$, choosing the same factor Ω one concludes again that $X^t\partial_t + X^r\partial_r$ is γ-causal in the metric (23) whenever it is in the metric g. Using again [5], in the region $r_- < r < r_+$, such a metric is conformal to a a flat two-dimensional metric on the interior of a diamond, with the conformal factor extending smoothly across those parts of its boundary where $r \to r_+$ or $r \to r_-$.

When $|a| < m$ the metric coefficients in γ extend analytically from the $(r > r_+)$ range to the $(r_- < r < r_+)$ range. As described in Sec. II, one can then smoothly glue together four diamonds as above to a single diamond on which $r_- < r < \infty$.

The singularity of γ at $r = 0$ reflects the fact that the metric g is singular at $\Sigma = 0$. This singularity persists even if $m = 0$, which might at first seem surprising since then there is no geometric singularity at $\Sigma = 0$ anymore [2]. However, this singularity of γ reflects the singularity of the associated coordinates on Minkowski space-time, with the set $r = 0$ in the projection metric corresponding to a boundary of the projection diagram.

For $r < 0$ we have $\Delta_r > 0$, and the inequality (20) still applies in the region where ∂_φ is spacelike. Here one needs

to keep in mind the nonempty *Carter time-machine* set [compare (17)]

$$\mathcal{V} := \{g_{\varphi\varphi} < 0\} = \Big\{ r \le 0, \Sigma \ne 0, \sin(\theta) \neq 0, \cos(2\theta) < -\frac{a^4 + 2a^2 m r + 3a^2 r^2 + 2r^4}{a^2 \Delta_r} \Big\}, \quad (25)$$

on which the Killing vector ∂_φ (which has 2π-periodic orbits) is timelike. The projection of the closure of this region to a two-dimensional diagram should be considered to be a singular set. But causality is restored regardless of the value of θ if we remove from $\mathcal{M}$ the closure of $\mathcal{V}$: Setting

$$\mathcal{U} := \mathcal{M} \setminus \overline{\mathcal{V}},$$

throughout $\mathcal{U}$ we have

$$\frac{a^4 + 2a^2 m r + 3a^2 r^2 + 2r^4}{a^2(a^2 - 2mr + r^2)} > 1 \iff r(a^2(2m + r) + r^3) > 0. \quad (26)$$

Equivalently,

$$r < \hat{r}_- := \frac{\sqrt[3]{\sqrt{3}\sqrt{a^6 + 27a^4 m^2} - 9a^2 m}}{3^{2/3}} - \frac{a^2}{\sqrt[3]{3}\sqrt[3]{\sqrt{3}\sqrt{a^6 + 27a^4 m^2} - 9a^2 m}} < 0; \quad (27)$$

see Fig. 2. In the region $r < \hat{r}_-$ the inequalities (19) hold again, and so the projected vector $\pi_*(X)$ as defined by (22) is causal, for g-causal X, in the metric γ given by (23). One concludes that the four-dimensional region $\{-\infty < r < r_-\}$ has the causal structure which projects to those diamonds of, e.g., Fig. 3 which contain a shaded region. Those shaded regions, which correspond both to the singularity $r = 0$, $\theta = \pi/2$ and to the time-machine region $\mathcal{V}$ of (25), belong to $\mathcal{W} = \pi(\mathcal{M})$ but *not* to $\pi(\mathcal{U})$. Causality within the shaded region is *not* represented in any useful way by a flat two-dimensional metric there, as causal curves can exit this region earlier, in Minkowskian time on the diagram, than they entered it. This results in causality violations throughout the enclosing diamond unless the shaded region is removed.

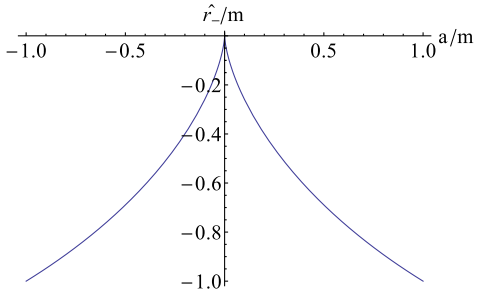

FIG. 2 (color online). The radius of the time-machine "left boundary" $\hat{r}_-/m$ as a function of a/m.

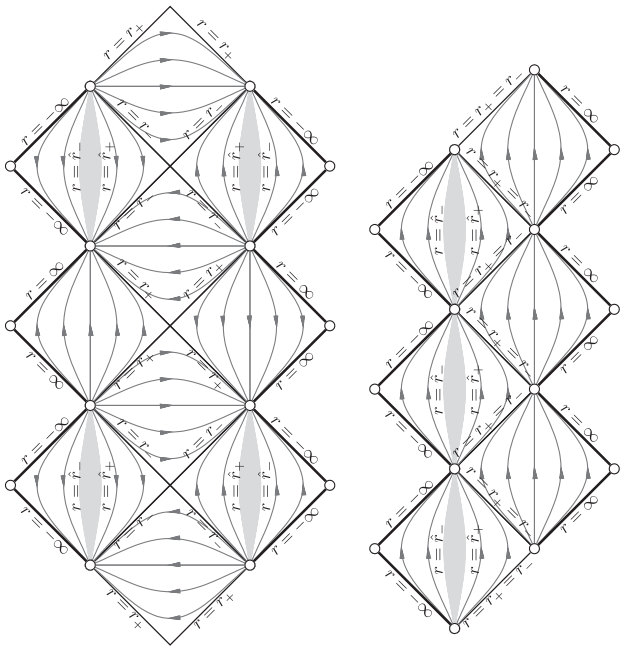

FIG. 3. A projection diagram for the Kerr-Newman metrics with two distinct zeros of Δ_r (left diagram) and one double zero (right diagram); see Remark III.1.

The projection diagrams for the usual maximal extensions of the Kerr-Newman metrics can be found in Fig. 3.

Remark III.1.—Let us make some general remarks concerning projection diagrams for the Kerr-Newman family of metrics, possibly with a nonvanishing cosmological constant Λ. The shaded regions in figures such as Fig. 3 and others contain the singularity $\Sigma = 0$ and the time-machine set $\{g_{\varphi\varphi} < 0\}$; they belong to the set $\mathcal{W} = \pi(\mathcal{M})$ but do *not* belong to the set $\pi(\mathcal{U})$, on which causality properties of two-dimensional Minkowski space-time reflect those of $\mathcal{U} \subset \mathcal{M}$. We emphasize that there are closed timelike curves through every point in the preimage under π of the entire diamonds containing the shaded areas. On the other hand, if the preimages of the shaded region are removed from $\mathcal{M}$, the causality relations in the resulting space-times are accurately represented by the diagrams, which are then proper.

The parameters $\hat{r}_\pm$ are determined by the mass and the charge parameters [see (64)], with $\hat{r}_+ = 0$ when the charge e vanishes and $\hat{r}_+$ positive otherwise. The boundaries $r = \pm\infty$ correspond to smooth conformal boundaries at infinity, with causal character determined by Λ. The arrows indicate the spatial or timelike character of the orbits of the isometry group. Maximal diagrams are obtained when continuing the diagrams shown in all allowed directions. It should be kept in mind that the resulting subsets of $\mathbb{R}^2$ are not simply connected in some cases, which implies that many alternative nonisometric maximal extensions of the

space-time can be obtained by taking various coverings of the planar diagram. One can also make use of the symmetries of the diagram to produce distinct quotients.■

1. Conformal diagrams for a class of two-dimensional submanifolds of Kerr space-time

One can find, e.g., in Refs. [1,3] conformal diagrams for the symmetry axes in the maximally extended Kerr space-time. These diagrams are identical with those of Fig. 3, except for the absence of shading. (The authors of Refs. [1,3] seem to indicate that the subset $r = 0$ plays a special role in their diagrams, which is not the case as the singularity $r = \cos\theta = 0$ does not intersect the symmetry axes.) Now, the symmetry axes are totally geodesic submanifolds, being the collection of fixed points of the isometry group generated by the rotational Killing vector field. They can be thought of as the submanifolds $\theta = 0$ and $\theta = \pi$ (with the remaining angular coordinate irrelevant then) of the extended Kerr space-time. As such, another totally geodesic two-dimensional submanifold in Kerr is the equatorial plane $\theta = \pi/2$, which is the set of fixed points of the isometry $\theta \mapsto \pi - \theta$. This leads one to inquire about the global structure of this submanifold or, more generally, of various families of two-dimensional submanifolds on which θ is kept fixed. The discussion that follows appears to have some interest of its own. More importantly for us, it illustrates clearly the distinction between projection diagrams, in which one projects out the θ and φ variables, and conformal diagrams for submanifolds where θ, and φ or the angular variable $\tilde{\varphi}$ of (30) below, are fixed.

An obvious family of two-dimensional Lorentzian submanifolds to consider is that of submanifolds, which we denote as $N_{\theta,\varphi}$, which are obtained by keeping θ and φ fixed. The metric, say $g(\theta)$, induced by the Kerr metric on $N_{\theta,\varphi}$ reads

$$g(\theta) = -\frac{\Delta_r - a^2\sin^2(\theta)}{\Sigma}dt^2 + \frac{\Sigma}{\Delta_r}dr^2 =: -F_1(r)dt^2 + \frac{dr^2}{F_2(r)}. \tag{28}$$

For $m^2 - a^2\cos^2(\theta) > 0$ the function F_1 has two first-order zeros at the intersection of $N_{\theta,\varphi}$ with the boundary of the ergoregion $\{g(\partial_t, \partial_t) > 0\}$:

$$r_{\theta,\pm} = m \pm \sqrt{m^2 - a^2\cos^2(\theta)}. \tag{29}$$

The key point is that these zeros are distinct from those of F_2 if $\cos^2\theta \neq 1$, which we assume in the remainder of this section. Since $r_{\theta,+}$ is larger than the largest zero of F_2, the metric $g(\theta)$ is *a priori* only defined for $r > r_{\theta,+}$. One checks that its Ricci scalar diverges as $(r - r_{\theta,+})^{-2}$ when $r_{\theta,+}$ is approached; therefore, those submanifolds do not extend smoothly across the ergosphere and will thus be of no further interest to us.

We consider, next, the two-dimensional submanifolds, say $\tilde{N}_{\theta,\tilde{\varphi}}$, of the Kerr space-time obtained by keeping θ and $\tilde{\varphi}$ fixed, where $\tilde{\varphi}$ is a new angular coordinate defined as

$$d\tilde{\varphi} = d\varphi + \frac{a}{\Delta_r}dr. \tag{30}$$

Using further the coordinate v defined as

$$dv = dt + \frac{(a^2 + r^2)}{\Delta_r}dr, \tag{31}$$

the metric, say $\tilde{g}(\theta)$, induced on $\tilde{N}_{\theta,\tilde{\varphi}}$ takes the form

$$\tilde{g}(\theta) = -\frac{\tilde{F}(r)}{\Sigma}dv^2 + 2dvdr = -\frac{\tilde{F}(r)}{\Sigma}dv\left(dv - 2\frac{\Sigma}{\tilde{F}(r)}dr\right), \tag{32}$$

where $\tilde{F}(r) := r^2 + a^2\cos^2(\theta) - 2mr$. The zeros of $\tilde{F}(r)$ are again given by (29). Setting

$$du = dv - 2\frac{\Sigma}{\tilde{F}(r)}dr \tag{33}$$

brings (32) to the form

$$\tilde{g}(\theta) = -\frac{\tilde{F}(r)}{\Sigma}dvdu.$$

The usual Kruskal-Szekeres type of analysis applies to this metric, leading to a conformal diagram as in the left Fig. 3 *with no shadings*, and with $r_{\pm}$ there replaced by $r_{\theta,\pm}$, *as long as* $\tilde{F}$ *has two distinct zeros*.

Several comments are in order.

First, the event horizons *within* $\tilde{N}_{\theta,\tilde{\varphi}}$ *do not* coincide with the intersection of the event horizons of the Kerr space-time with $\tilde{N}_{\theta,\tilde{\varphi}}$. This is not difficult to understand by noting that the class of causal curves that lie within $\tilde{N}_{\theta,\tilde{\varphi}}$ is smaller than the class of causal curves in space-time, and there is therefore no *a priori* reason to expect that the associated horizons will be the same. In fact, is should be clear that the event horizons within $\tilde{N}_{\theta,\tilde{\varphi}}$ should be located on the boundary of the ergoregion, since in two space-time dimensions the boundary of an ergoregion is necessarily a null hypersurface. This illustrates the fact that conformal diagrams for submanifolds might fail to represent correctly the location of horizons. The reason that the conformal diagrams for the symmetry axes correctly reflect the global structure of the space-time is an accident related to the fact that the ergosphere touches the event horizon there.

This last issue acquires a dramatic dimension for extreme Kerr black holes, for which $|a| = m$, where for $\theta \in (0, \pi)$ the global structure of maximally extended $\tilde{N}_{\theta,\tilde{\varphi}}$'s is represented by an unshaded version of the left Fig. 3, while the conformal diagrams for the axisymmetry axes are given by the unshaded version of the right Fig. 3.

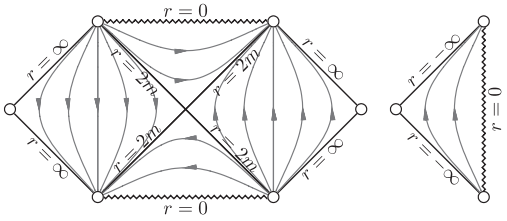

FIG. 4. The conformal diagram of a maximal analytic extension of the equatorial plane $\theta = \pi/2$ and constant $\tilde{\varphi}$ for Kerr metrics with arbitrary $a \in \mathbb{R}$ with $r > 0$ (left) and $r < 0$ (right).

Next, another dramatic change arises in the global structure of the $\tilde{N}_{\theta,\tilde{\varphi}}$'s with $\theta = \pi/2$. Indeed, in this case we have $r_{\theta,+} = 2m$, as in Schwarzschild space-time, and $r_{\theta,-} = 0$, regardless of whether the metric is underspinning, extreme, or overspinning. Since $r_{\theta,-}$ coincides now with the location of the singularity, $\tilde{N}_{\theta,\tilde{\varphi}}$ acquires two connected components: one where $r > 0$ and a second one with $r < 0$. The conformal diagram of the first one is identical to that of the Schwarzschild space-time with positive mass, while the second is identical to that of Schwarzschild with negative mass; see Fig. 4. We thus obtain the unexpected conclusion that the singularity $r = \cos(\theta) = 0$ has a spacelike character when approached with positive r within the equatorial plane and a timelike one when approached with negative r within that plane. This is rather obvious in retrospect, since the metric induced by Kerr on $\tilde{N}_{\pi/2,\tilde{\varphi}}$ coincides, when $m > 0$, with the one induced by the Schwarzschild metric with positive mass in the region $r > 0$ and with the Schwarzschild metric with negative mass $-m$ in the region $r < 0$.

Note finally that, surprisingly enough, even for overspinning Kerr metrics there will be a range of angles θ near $\pi/2$ so that $\tilde{F}$ will have two distinct first-order zeros. This implies that, for such θ, the global structure of maximally extended $\tilde{N}_{\theta,\tilde{\varphi}}$'s will be similar to that of the corresponding submanifolds of the underspinning Kerr solutions. This should be compared with the projection diagram for overspinning Kerr space-times, to be found in Fig. 5.

2. The orbit space-metric on $\mathcal{M}/\mathrm{U}(1)$

Let h denote the tensor field obtained by quotienting out in the Kerr metric g the $\eta := \partial_\varphi$ direction:

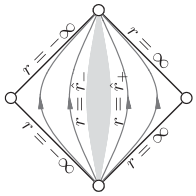

FIG. 5. A projection diagram for overspinning Kerr-Newman space-times.

$$h(X, Y) = g(X, Y) - \frac{g(X, \eta)g(Y, \eta)}{g(\eta, \eta)}. \tag{34}$$

The tensor field h projects to the natural quotient metric on the manifold part of $\mathcal{M}/\mathrm{U}(1)$. In the region where η is spacelike, the quotient space $\mathcal{M}/\mathrm{U}(1)$ has the natural structure of a manifold with boundary, where the boundary is the image, under the quotient map, of the axis of rotation

$$\mathcal{A} := \{\eta = 0\}.$$

Using t, r, θ as coordinates on the quotient space we find a diagonal metric

$$h = h_{tt}dt^2 + \frac{\Sigma}{\Delta_r}dr^2 + \Sigma d\theta^2, \tag{35}$$

where

$$h_{tt} = g_{tt} - \frac{g_{t\varphi}^2}{g_{\varphi\varphi}},$$

as in (18). Thus, the metric γ of Sec. III C is directly constructed out of the (t, r) part of the quotient-space metric h. However, the analogy is probably misleading as there does not seem to be any direct correspondence between the quotient space $\mathcal{M}/\mathrm{U}(1)$ and the natural manifold as constructed in Sec. III C using the metric γ [10].

D. The Kerr-Newman metrics

The analysis of the Kerr-Newman metrics is essentially identical: The metric takes the same general form (15), except that now

$$\Delta_r = r^2 + a^2 + e^2 - 2mr =: (r - r_+)(r - r_-),$$

and we assume that $e^2 + a^2 \leq m$ so that the roots are real. We have

$$g_{\varphi\varphi} = \frac{\sin^2(\theta)((r^2 + a^2)^2 - a^2\Delta_r\sin^2(\theta))}{\Sigma}, \tag{36}$$

$$g_{tt} - \frac{g_{t\varphi}^2}{g_{\varphi\varphi}} = -\frac{\Delta_r\Sigma}{(r^2 + a^2)^2 - a^2\Delta_r\sin^2(\theta)}, \tag{37}$$

and note that the sign of the denominator in (37) coincides with the sign of $g_{\varphi\varphi}$. Hence

$$\mathrm{sgn}\left(g_{tt} - \frac{g_{t\varphi}^2}{g_{\varphi\varphi}}\right) = -\mathrm{sgn}(\Delta_r)\mathrm{sgn}(g_{\varphi\varphi}).$$

For $g_{\varphi\varphi} > 0$, which is the main region of interest, we conclude that the minimum of $(g_{tt} - \frac{g_{t\varphi}^2}{g_{\varphi\varphi}})\Sigma^{-1}\Delta_r^{-1}$ is assumed at $\theta = \frac{\pi}{2}$ and the maximum at $\theta = 0, \pi$, so for all r for which $g_{\varphi\varphi} > 0$ we have

$$-\frac{\Delta_r\Sigma}{(r^2 + a^2)^2 - a^2\Delta_r} \leq g_{tt} - \frac{g_{t\varphi}^2}{g_{\varphi\varphi}} \leq -\frac{\Delta_r\Sigma}{(r^2 + a^2)^2}. \tag{38}$$

Choosing the conformal factor as

$$\Omega^2 = \frac{r^2 + a^2}{\Sigma}$$

we obtain, for g-causal vectors X,

$$\begin{aligned} 0 \geq \Omega^2 g(X,X) &= \Omega^2 g_{\mu\nu} X^\mu X^\nu \\ &\geq \Omega^2 \left(g_{tt} - \frac{g_{t\varphi}^2}{g_{\varphi\varphi}} \right) (X^t)^2 + \Omega^2 g_{rr} (X^r)^2 \\ &\geq -\frac{\Delta_r (r^2 + a^2)}{(r^2 + a^2)^2 - a^2 \Delta_r} (X^t)^2 + \frac{(r^2 + a^2)}{\Delta_r} (X^r)^2. \end{aligned} \tag{39}$$

This leads to the following projection metric:

$$\begin{aligned} \gamma &:= -\frac{\Delta_r (r^2 + a^2)}{(r^2 + a^2)^2 - a^2 \Delta_r} dt^2 + \frac{(r^2 + a^2)}{\Delta_r} dr^2 \\ &= -\frac{\Delta_r (r^2 + a^2)}{a^2 (r(2m + r) - e^2) + r^4} dt^2 + \frac{(r^2 + a^2)}{\Delta_r} dr^2, \end{aligned} \tag{40}$$

which is Lorentzian if and only if r is such that $g_{\varphi\varphi} > 0$ for all $\theta \in [0, \pi]$. Now, it follows from (36) that $g_{\varphi\varphi}$ will have the *wrong* sign if

$$0 > (r^2 + a^2)^2 - a^2 \Delta_r \sin^2(\theta). \tag{41}$$

This does not happen when $\Delta_r \leq 0$, and hence in a neighborhood of both horizons. On the other hand, for $\Delta_r > 0$, a necessary condition for (41) is

$$\begin{aligned} 0 &> (r^2 + a^2)^2 - a^2 \Delta_r \\ &= r^4 + r^2 a^2 + 2mra^2 - a^2 e^2 =: f(r). \end{aligned} \tag{42}$$

The second derivative of f is positive; hence, f' has exactly one real zero. Note that f is strictly smaller than the corresponding function for the Kerr metric, where $e = 0$; thus, the interval where f is negative encloses the corresponding interval for Kerr. We conclude that f is negative on an interval $(\hat{r}_-, \hat{r}_+)$, with $\hat{r}_- < 0 < \hat{r}_+ < r_-$.

The corresponding projection diagrams are identical to those of the Kerr space-time, see Fig. 3, with the minor modification that the region to be excised from the diagram is $\{r \in (\hat{r}_-, \hat{r}_+)\}$, with now $\hat{r}_+ > 0$, while we had $\hat{r}_+ = 0$ in the uncharged case.

E. The Kerr-de Sitter metrics

The Kerr-de Sitter metric in Boyer-Lindquist-like coordinates reads [12,13]

$$\begin{aligned} g = &\frac{\Sigma}{\Delta_r} dr^2 + \frac{\sin^2(\theta)}{\Xi^2 \Sigma} \Delta_\theta (a dt - (r^2 + a^2) d\varphi)^2 \\ &- \frac{1}{\Xi^2 \Sigma} \Delta_r (dt - a \sin^2(\theta) d\varphi)^2 + \frac{\Sigma}{\Delta_\theta} d\theta^2, \end{aligned} \tag{43}$$

where

$$\begin{aligned} \Sigma &= r^2 + a^2 \cos^2(\theta), \\ \Delta_r &= (r^2 + a^2) \left(1 - \frac{\Lambda}{3} r^2 \right) - 2\mu \Xi r, \end{aligned} \tag{44}$$

and

$$\Delta_\theta = 1 + \frac{\Lambda}{3} a^2 \cos^2(\theta), \qquad \Xi = 1 + \frac{\Lambda}{3} a^2, \tag{45}$$

for some real parameters a and μ, where Λ is the cosmological constant. In this section we assume $\Lambda > 0$ and $a \neq 0$. By a redefinition $\varphi \mapsto -\varphi$ we can always achieve $a > 0$, similarly changing r to $-r$ if necessary we can assume that $\mu \geq 0$. The case $\mu = 0$ leads to the de Sitter metric in unusual coordinates (see, e.g., Eq. (17) in Ref. [14]). The inequalities $a > 0$ and $\mu > 0$ will be assumed from now on.

The Lorentzian character of the metric should be clear from (43); alternatively, one can calculate the determinant of g:

$$\det(g) = -\frac{\Sigma^2}{\Xi^4} \sin^2\theta. \tag{46}$$

We have

$$g^{tt} = \frac{g_{rr} g_{\theta\theta} g_{\varphi\varphi}}{\det(g)} = -\frac{\Xi^4}{\Delta_\theta} \times \frac{1}{\Delta_r} \times \frac{g_{\varphi\varphi}}{\sin^2\theta}, \tag{47}$$

which shows that either t or its negative is a time function whenever Δ_r and $g_{\varphi\varphi}/\sin^2\theta$ are positive. (Incidentally, chronology is violated on the set where $g_{\varphi\varphi} < 0$; we will return to this shortly.) One also has

$$g^{rr} = \frac{\Delta_r}{\Sigma}, \tag{48}$$

which shows that r or its negative is a time function in the region where $\Delta_r < 0$.

The character of the principal orbits of the isometry group $\mathbb{R} \times U(1)$ is determined by the sign of the determinant

$$\det \begin{pmatrix} g_{tt} & g_{\varphi t} \\ g_{\varphi t} & g_{\varphi\varphi} \end{pmatrix} = -\frac{\Delta_r \Delta_\theta}{\Xi^4} \sin^2\theta. \tag{49}$$

Therefore, for $\sin(\theta) \neq 0$ the orbits are two-dimensional, timelike in the regions where $\Delta_r > 0$, spacelike where $\Delta_r < 0$, and null where $\Delta_r = 0$ once the space-time has been appropriately extended to include the last set.

When $\mu \neq 0$ the set $\{\Sigma = 0\}$ corresponds to a geometric singularity in the metric. To see this, note that

$$g(\partial_t, \partial_t) = \frac{a^2 \sin^2\theta \Delta_\theta - \Delta_r}{\Sigma \Xi^2} = 2\frac{\mu r}{\Sigma \Xi} + O(1), \tag{50}$$

where $O(1)$ denotes a function which is bounded near $\Sigma = 0$. It follows that for $\mu \neq 0$ the norm of the Killing vector ∂_t blows up as the set $\{\Sigma = 0\}$ is approached along

the plane $\cos(\theta) = 0$, which would be impossible if the metric could be continued across this set in a C^2 manner.

The function Δ_r has exactly two distinct first-order real zeros when

$$\mu^2 > \frac{2}{3^5\Xi^2\Lambda}(3 - a^2\Lambda)^3. \tag{51}$$

It has at least two, and up to four, possibly but not necessarily distinct, real roots when

$$a^2\Lambda \leq 3, \qquad \mu^2 \leq \frac{2}{3^5\Xi^2\Lambda}(3 - a^2\Lambda)^3. \tag{52}$$

The negative root r_1 is always simple and negative; the remaining ones are positive. We can thus order the roots as

$$r_1 < 0 < r_2 \leq r_3 \leq r_4, \tag{53}$$

when there are four real ones, and we set $r_3 \equiv r_4 := r_2$ when there are only two real roots $r_1 < r_2$. The function Δ_r is positive for $r \in (r_1, r_2)$, and for $r \in (r_3, r_4)$ whenever the last interval is not empty; Δ_r is negative or vanishing otherwise.

It holds that

$$g_{\varphi\varphi} = \frac{\sin^2(\theta)(\Delta_\theta(r^2 + a^2)^2 - a^2\Delta_r\sin^2(\theta))}{\Xi^2\Sigma} \tag{54}$$

$$= \frac{\sin^2(\theta)}{\Xi}\left(\frac{2a^2\mu r\sin^2(\theta)}{a^2\cos^2(\theta) + r^2} + a^2 + r^2\right). \tag{55}$$

The second line is manifestly non-negative for $r \geq 0$ and positive there away from the axis $\sin(\theta) = 0$. The first line is manifestly non-negative for $\Delta_r \leq 0$, and hence also in a neighborhood of this set.

Next

$$g_{tt} - \frac{g_{t\varphi}^2}{g_{\varphi\varphi}} = -\frac{\Delta_\theta\Delta_r\Sigma}{\Xi^2(\Delta_\theta(r^2 + a^2)^2 - \Delta_r a^2\sin^2(\theta))} = -\frac{\Delta_\theta\Delta_r\Sigma}{\Xi^2(A(r) + B(r)\cos(2\theta))}, \tag{56}$$

with

$$A(r) = \frac{\Xi}{2}(a^4 + 3a^2r^2 + 2r^4 + 2a^2\mu r), \tag{57}$$

$$B(r) = \frac{a^2}{2}\Xi(a^2 + r^2 - 2\mu r). \tag{58}$$

We have

$$A(r) + B(r) = \Xi(a^2 + r^2)^2, \qquad A(r) - B(r) = r^2\Xi\left(a^2 + r^2 + 2\frac{a^2\mu}{r}\right), \tag{59}$$

which confirms that for $r > 0$, or for large negative r, we have $A > |B| > 0$, as needed for $g_{\varphi\varphi} \geq 0$. The function

$$f(r, \theta) := \frac{(A(r) + B(r)\cos(2\theta))}{\Delta_\theta} \equiv \frac{(A(r) + B(r)\cos(2\theta))}{1 + \frac{\Lambda}{3}a^2\cos^2(\theta)}$$

satisfies

$$\frac{\partial f}{\partial\theta} = -\frac{a^2\Xi}{\Delta_\theta^2}\Delta_r\sin(2\theta), \tag{60}$$

which has the same sign as $-\Delta_r\sin(2\theta)$. In any case, its extrema are achieved at $\theta = 0$, $\pi/2$ and π. Accordingly, this is where the extrema of the right-hand side of (56) are achieved as well. In particular, for $\Delta_r > 0$, we find

$$\frac{\Delta_r\Sigma}{(a^2 + r^2)^2} \leq \Xi^2\left|g_{tt} - \frac{g_{t\varphi}^2}{g_{\varphi\varphi}}\right| \leq \frac{\Sigma\Delta_r}{\Xi r(a^2(2\mu + r) + r^3)}, \tag{61}$$

with the minimum attained at $\theta = 0$ and the maximum attained at $\theta = \pi/2$.

To obtain the projection diagram, we can now repeat word for word the analysis carried out for the Kerr metrics on the set $\{g_{\varphi\varphi} > 0\}$. Choosing a conformal factor Ω^2 equal to

$$\Omega^2 = \frac{r^2 + a^2}{\Sigma}, \tag{62}$$

one is led to a projection metric

$$\gamma := -\frac{(r^2 + a^2)\Delta_r}{\Xi^3 r(a^2(2\mu + r) + r^3)}dt^2 + \frac{r^2 + a^2}{\Delta_r}dr^2. \tag{63}$$

It remains to understand the set

$$\mathcal{V} := \{g_{\varphi\varphi} < 0\},$$

where $g_{\varphi\varphi}$ is negative. To avoid repetitiveness, we will do it simultaneously both for the charged and the uncharged case, where (54) still applies [but not (55) for $e \neq 0$] with Δ_r given by (64); the Kerr-de Sitter case is obtained by setting $e = 0$ in what follows. A calculation shows that $g_{\varphi\varphi}$ is the product of a non-negative function with

$$\chi := 2a^2\mu r - a^2e^2 + r^2a^2 + r^4 + (r^2a^2 - 2a^2\mu r + a^2e^2 + a^4)\cos^2(\theta).$$

This is clearly positive for all r and all $\theta \neq \pi/2$ when $\mu = e = 0$, which shows that $\mathcal{V} = \varnothing$ in this case.

Next, the function χ is sandwiched between the two following functions of r, obtained by setting $\cos(\theta) = 0$ or $\cos^2(\theta) = 1$ in χ:

$$\chi_0 := r^4 + r^2a^2 + 2a^2\mu r - a^2e^2, \quad \chi_1 := (r^2 + a^2)^2.$$

Hence, χ is positive for all r when $\cos^2(\theta) = 1$. Next, for $\mu > 0$ the function χ_0 is negative for negative r near zero. Further, χ_0 is convex. We conclude that, for $\mu > 0$, the set on which χ_0 is nonpositive is a nonempty interval $[\hat{r}_-, \hat{r}_+]$ containing the origin. We have already seen that $g_{\varphi\varphi}$ is non-negative wherever $\Delta_r \leq 0$, and since $r_2 > 0$ we must have

$$r_1 < \hat{r}_- \leq \hat{r}_+ < r_2.$$

In fact, when $e = 0$ the value of $\hat{r}_-$ is given by (27) with m there replaced by μ, with $\hat{r}_- = 0$ if and only if $\mu = 0$.

We conclude that if $\mu = e = 0$ the time-machine set is empty, while if $|\mu| + e^2 > 0$ there are always causality violations "produced" in the nonempty region $\{\hat{r}_- \le r \le \hat{r}_+\}$.

The projection diagrams for the Kerr-Newman-de Sitter family of metrics depend upon the number of zeros of Δ_r, and their nature, and can be found in Figs. 6–9.

F. The Kerr-Newman-de Sitter metrics

In the standard Boyer-Lindquist coordinates the Kerr-Newman-de Sitter metric takes the form (43) [13,15,16] with all the functions as in (44) and (45) except for Δ_r, which instead takes the form

$$\Delta_r = \left(1 - \frac{1}{3}\Lambda r^2\right)(r^2 + a^2) - 2\Xi\mu r + \Xi e^2, \qquad (64)$$

where $\sqrt{\Xi}e$ is the electric charge of the space-time. In this section we assume,

$$\Lambda > 0, \qquad \mu \ge 0, \qquad a > 0, \qquad e \ne 0.$$

The calculations of the previous section, and the analysis of zeros of Δ_r, remain identical except for the following equations: First,

$$g_{\varphi\varphi} = \frac{\sin^2(\theta)}{\Xi}\left(\frac{a^2(2\mu r - e^2)\sin^2(\theta)}{a^2\cos^2(\theta) + r^2} + a^2 + r^2\right), \qquad (65)$$

the sign of which requires further analysis; we will return to this shortly. Next, we still have

$$g_{tt} - \frac{g_{t\varphi}^2}{g_{\varphi\varphi}} = -\frac{\Delta_\theta \Delta_r \Sigma}{\Xi^2(\Delta_\theta(r^2 + a^2)^2 - \Delta_r a^2 \sin^2(\theta))} = -\frac{\Delta_\theta \Delta_r \Sigma}{\Xi^2(A(r) + B(r)\cos(2\theta))}, \qquad (66)$$

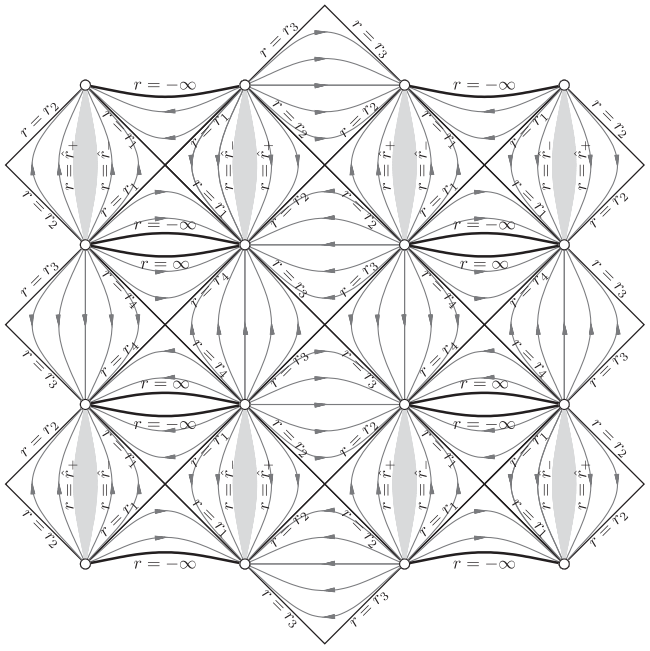

FIG. 6. A projection diagram for the Kerr-Newman-de Sitter metric with four distinct zeros of Δ_r; see Remark III.1.

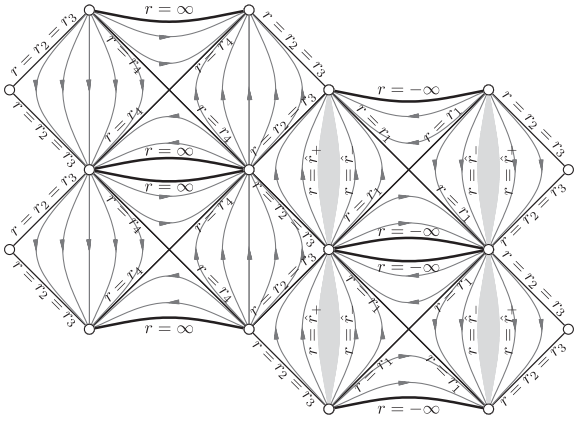

FIG. 7. A projection diagram for the Kerr-Newman-de Sitter metrics with three distinct zeros of Δ_r, $r_1 < 0 < r_2 = r_3 < r_4$; see Remark III.1.

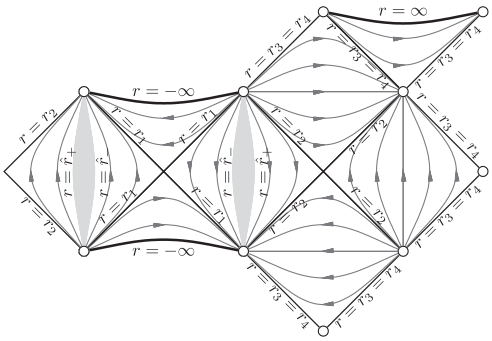

FIG. 8. A projection diagram for the Kerr-Newman-de Sitter metrics with three distinct zeros of Δ_r, $r_1 < 0 < r_2 < r_3 = r_4$; see Remark III.1. Note that one cannot continue the diagram simultaneously across all boundaries $r = r_3$ on $\mathbb{R}^2$, but this can be done on an appropriate Riemann surface.

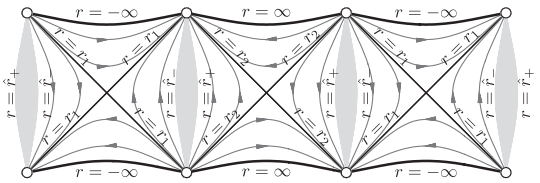

FIG. 9. A projection diagram for the Kerr-Newman-de Sitter metrics with two distinct first-order zeros of Δ_r, $r_1 < 0 < r_2$ and $\mu > 0$; see Remark III.1. The diagram for a first-order zero at r_1 and third-order zero at $r_2 = r_3 = r_4$ would be identical except for the bifurcation surface of the bifurcate Killing horizon at the intersection of the lines $r = r_2$, which does not exist in the third-order case and has therefore to be removed from the diagram.

but now

$$A(r) = \frac{\Xi}{2}(a^4 + 3a^2r^2 + 2r^4 + 2a^2\mu r - a^2e^2),$$

$$B(r) = \frac{a^2}{2}\Xi(a^2 + r^2 - 2\mu r + e^2),$$

with

$$A(r) + B(r) = \Xi(a^2 + r^2)^2,$$

$$A(r) - B(r) = r^2\Xi\left(a^2 + r^2 + 2\frac{a^2\mu}{r} - \frac{a^2e^2}{r^2}\right).$$

Equation (60) remains unchanged, and for $\Delta_r > 0$, we find

$$\frac{\Delta_r\Sigma}{(a^2 + r^2)^2} \le \Xi^2\left| g_{tt} - \frac{g_{t\varphi}^2}{g_{\varphi\varphi}}\right| \le \frac{\Sigma\Delta_r}{\Xi(a^2(2\mu r - e^2 + r^2) + r^4)}, \quad (67)$$

with the minimum attained at $\theta = 0$ and the maximum attained at $\theta = \pi/2$. This leads to the projection metric

$$\gamma := -\frac{\Delta_r}{\Xi^3(a^2(2\mu r - e^2 + r^2) + r^4)}dt^2 + \frac{1}{\Delta_r}dr^2. \quad (68)$$

We recall that the analysis of the time-machine set $\{g_{\varphi\varphi} < 0\}$ has already been carried out at the end of Sec. III E, where it was shown that for $e \neq 0$ causality violations always exist and arise from the nonempty region $\{\hat{r}_- \le r \le \hat{r}_+\}$.

The projection diagrams for the Kerr-Newman-de Sitter family of metrics can be found in Figs. 6–9.

G. The Kerr-Newman-anti de Sitter metrics

We consider the metric (43)–(45), with however Δ_r given by (64), assuming that

$$a^2 + e^2 > 0, \qquad \Lambda < 0.$$

While the local calculations carried out in Sec. III E remain unchanged, one needs to reexamine the occurrence of zeros of Δ_r.

We start by noting that the requirement that $\Xi \neq 0$ imposes

$$1 + \frac{\Lambda}{3}a^2 \neq 0.$$

Next, a negative Ξ would lead to a function Δ_θ which changes sign. By inspection, one finds that the signature changes from $(- + ++)$ to $(+ - --)$ across these zeros, which implies nonexistence of a coordinate system in which the metric could be smoothly continued there [17]. From now on we thus assume that

$$\Xi \equiv 1 + \frac{\Lambda}{3}a^2 > 0. \quad (69)$$

It is well known that those metrics for which Δ_r has no zeros are nakedly singular whenever

$$e^2 + |\mu| > 0. \quad (70)$$

This can, in fact, be easily seen from the following formula for g_{tt} on the equatorial plane:

$$g_{tt} = \frac{1}{3\Xi^2r^2}(-3\Xi e^2 + 6\Xi\mu r + (\Lambda a^2 - 3)r^2 + \Lambda r^4). \quad (71)$$

So, under (70) the norm of the Killing vector ∂_t is unbounded and the metric cannot be C^2-continued across $\{\Sigma = 0\}$ by usual arguments.

Turning our attention, first, to the region where $r > 0$, the occurrence of zeros of Δ_r requires that

$$\mu \ge \mu_c(a, e, \Lambda) > 0.$$

Hence, there is a positive threshold for the mass of a black hole at given a and e. The solution with $\mu = \mu_c$ has the property that Δ_r and its r derivative have a joint zero and can thus be found by equating to zero the resultant of these two polynomials in r. An explicit formula for $m_c = \Xi\mu_c$ can be given, which takes a relatively simple form when expressed in terms of suitably renormalized parameters. We set

$$\alpha = \sqrt{\frac{|\Lambda|}{3}}a \Longleftrightarrow a = \alpha\sqrt{\frac{3}{|\Lambda|}},$$

$$\beta = \frac{3\sqrt{|\Lambda|}}{(1 + \alpha^2)^{3/2}}\mu\Xi \Longleftrightarrow m := \Xi\mu = \frac{(1 + \alpha^2)^{3/2}}{3\sqrt{|\Lambda|}}\beta,$$

and

$$\gamma = 9\frac{\alpha^2 + \frac{|\Lambda|}{3}q^2}{(1 + \alpha^2)^2}$$

$$\Longleftrightarrow q^2 := \Xi e^2 = \frac{3}{|\Lambda|}\left(\left(\frac{1 + \alpha^2}{3}\right)^2\gamma - \alpha^2\right).$$

Letting β_c be the value of β corresponding to μ_c, one finds

$$\beta_c = \frac{\sqrt{-9 + 36\gamma + \sqrt{3}\sqrt{(3 + 4\gamma)^3}}}{3\sqrt{2}}$$

$$\Longleftrightarrow m_c^2 = \frac{(1 + \alpha^2)^3(-9 + 36\gamma + \sqrt{3}\sqrt{(3 + 4\gamma)^3})}{162|\Lambda|}. \quad (72)$$

When $q = 0$, the graph of β_c as a function of α can be found in Fig. 10. In general, the graph of β_c as a function of a and q can be found in Fig. 11.

Note that if $q = 0$, then γ can be used as a replacement for a; otherwise, γ is a substitute for q at fixed a.

When $e = 0$ we have $m_c = a + O(a^3)$ for small a, and $m_c \to \frac{8}{3\sqrt{|\Lambda|}}$ as $|a| \nearrow \sqrt{|3/\Lambda|}$.

According to Ref. [18], the physically relevant mass of the solution is μ and *not* m; because of the rescaling involved, we have $\mu_c \to \infty$ as $|a| \nearrow \sqrt{|3/\Lambda|}$.

We have $d^2\Delta_r/dr^2 > 0$, so that the set $\{\Delta_r \le 0\}$ is an interval (r_-, r_+), with $0 < r_- < r_+$.

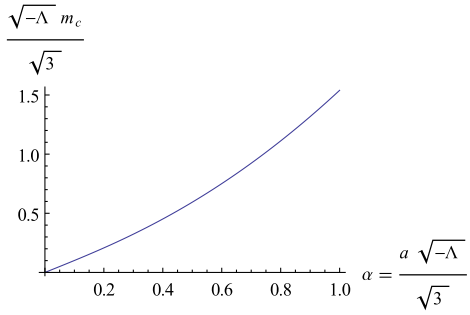

FIG. 10 (color online). The critical mass parameter $m_c\sqrt{|\Lambda/3|} = \Xi\mu_c\sqrt{|3/\Lambda|}$ as a function of $|a|\sqrt{|\Lambda/3|}$ when $q = 0$.

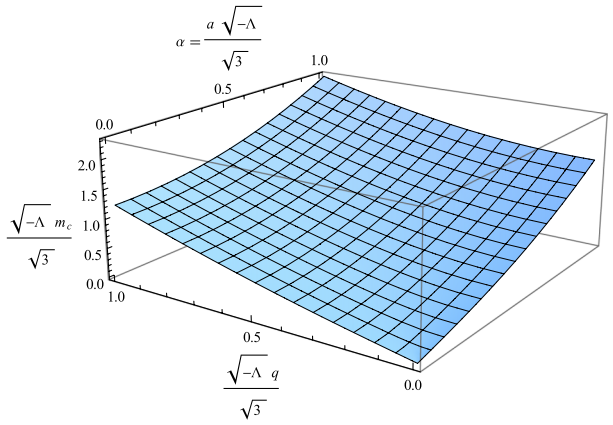

FIG. 11 (color online). The critical mass parameter $m_c\sqrt{\frac{|\Lambda|}{3}}$ as a function of $\alpha = a\sqrt{\frac{|\Lambda|}{3}}$ and $q\sqrt{\frac{|\Lambda|}{3}}$.

It follows from (54) that $g_{\varphi\varphi}/\sin^2(\theta)$ is positive for $r > 0$, and the analysis of the time-machine set is identical to the case $\Lambda > 0$ as long as $\Xi > 0$, which is assumed. We note that stable causality of each region on which Δ_r has constant sign follows from (47) and (48).

The projection metric is formally identical to that derived in Sec. III E, with projection diagrams seen in Fig. 12.

H. The Emparan-Reall metrics

We consider the Emparan-Reall black-ring metric as presented in [19]:

$$ds^2 = -\frac{F(y)}{F(x)}\left(dt - CR\frac{1+y}{F(y)}d\psi\right)^2 + \frac{R^2F(x)}{(x-y)^2} \times\left[-\frac{G(y)}{F(y)}d\psi^2 - \frac{dy^2}{G(y)} + \frac{dx^2}{G(x)} + \frac{G(x)}{F(x)}d\phi^2\right], \tag{73}$$

where

$$F(\xi) = 1 + \lambda\xi, \qquad G(\xi) = (1-\xi^2)(1+\nu\xi), \tag{74}$$

and

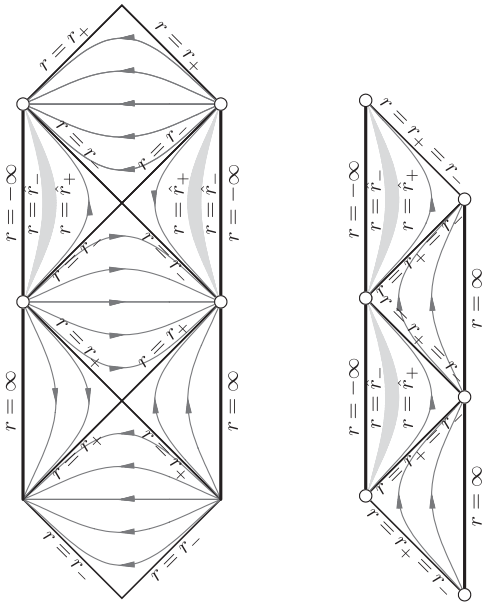

FIG. 12. The projection diagrams for the Kerr-Newman-anti de Sitter metrics with two distinct zeros of Δ_r (left diagram) and one double zero (right diagram); see Remark III.1.

$$C = \sqrt{\lambda(\lambda-\nu)\frac{1+\lambda}{1-\lambda}}. \tag{75}$$

The parameter λ is chosen to be

$$\lambda = \frac{2\nu}{1+\nu^2}, \tag{76}$$

with the parameter ν lying in (0, 1), so that

$$0 < \nu < \lambda < 1. \tag{77}$$

The coordinates x, y lie in the ranges $-\infty \le y \le -1$, $-1 \le x \le 1$, assuming further that $(x, y) \ne (-1, -1)$. The event horizons are located at $y = y_h = -1/\nu$ and the ergosurface is at $y = y_e = -1/\lambda$. The ∂_ψ axis is at $y = -1$ and the ∂_ϕ axis is split into two parts $x = \pm 1$. Spatial infinity i^0 corresponds to $x = y = -1$. The metric becomes singular as $y \to -\infty$.

Although this is not immediately apparent from the current form of the metric, it is known [20] that ∂_ψ is spacelike or vanishing in the region of interest, with $g_{\psi\psi} > 0$ away from the rotation axis $y = -1$. Now, the metric (73) may be rewritten in the form

$$g = \left(g_{tt} - \frac{g_{t\psi}^2}{g_{\psi\psi}}\right)dt^2 - \frac{R^2}{(x-y)^2}\frac{F(x)}{G(y)}dy^2 + \underbrace{g_{\psi\psi}\left(d\psi + \frac{g_{t\psi}}{g_{\psi\psi}}dt\right)^2}_{\ge 0} + g_{xx}dx^2 + g_{\phi\phi}d\phi^2. \tag{78}$$

We have

$$g_{tt} - \frac{g_{t\psi}^2}{g_{\psi\psi}} = -\frac{G(y)F(y)F(x)}{F(x)^2G(y) + C^2(1+y)^2(x-y)^2}. \quad (79)$$

It turns out that there is a nonobvious factorization of the denominator as

$$F(x)^2G(y) + C^2(1+y)^2(x-y)^2 = -F(y)I(x,y),$$

where I is a second-order polynomial in x and y with coefficients depending upon ν, sufficiently complicated so that it cannot be usefully displayed here. The polynomial I turns out to be non-negative, which can be seen using a trick similar to one in Ref. [21], as follows: One introduces new, non-negative, variables and parameters (X, Y, σ) via the equations

$$x = X - 1, \qquad y = -Y - 1, \qquad \nu = \frac{1}{1+\sigma}, \quad (80)$$

with $0 \le X \le 2$, $0 \le Y < +\infty$, $0 < \sigma < +\infty$. A MATHEMATICA calculation shows that in this parameterization the function I is a rational function of the new variables, with a simple denominator which is explicitly non-negative, while the numerator is a complicated polynomial in X, Y, σ with, however, *all coefficients positive*.

Let $\Omega = (x-y)/\sqrt{F(x)}$, then the function

$$\kappa(x,y) := \Omega^2\left(g_{tt} - \frac{g_{t\psi}^2}{g_{\psi\psi}}\right) = -\frac{G(y)F(y)}{\frac{F(x)^2}{(x-y)^2}G(y) + C^2(1+y)^2} \quad (81)$$

has extrema in x only for $x = y = -1$ and $x = -1/\lambda < -1$. This may be seen from its derivative with respect to x, which is explicitly nonpositive in the ranges of variables of interest:

$$\frac{\partial\kappa}{\partial x} = -\frac{2G(y)^2F(y)^2F(x)(x-y)}{(F(x)^2G(y) + C^2(1+y)^2(x-y)^2)^2} = -\frac{2G(y)^2F(x)(x-y)}{I(x,y)^2}.$$

Therefore,

$$\frac{(1+y)^2G(y)}{I(-1,y)} = \kappa(-1,y) \ge \kappa(x,y) \ge \kappa(1,y) = \frac{(1-y)^2G(y)}{I(1,y)}.$$

Since both $I(-1,y)$ and $I(1,y)$ are positive, in the domain of outer communications $\{-1/\nu < y \le -1\}$ where $G(y)$ is negative we obtain

$$\frac{-G(y)(1+y)^2}{I(-1,y)} \le \left|\Omega^2\left(g_{tt} - \frac{g_{t\psi}^2}{g_{\psi\psi}}\right)\right| \le \frac{-G(y)(1-y)^2}{I(1,y)}. \quad (82)$$

One finds

$$I(1,y) = \frac{1+\lambda}{1-\lambda}(-1+y^2)(1 - y(\lambda-\nu) - \lambda\nu),$$

which leads to the projection metric

$$\gamma := \chi(y)\frac{G(y)}{(-1-y)}dt^2 - \frac{R^2}{G(y)}dy^2, \quad (83)$$

where, using the variables (80) to make manifest the positivity of χ in the range of variables of interest,

$$\chi(y) = \frac{(1-y)(1-\lambda)}{(1+\lambda)(1-y(\lambda-\nu)-\lambda\nu)} = \frac{(2+Y)\sigma(1+\sigma)(2+2\sigma+\sigma^2)}{(2+\sigma)^3(2+Y+\sigma)} > 0.$$

The calculation of (3) leads to the following conformal metric:

$$\overset{(2)}{g} = R\sqrt{\frac{\chi}{|1+y|}}(-\hat{F}dt^2 + \hat{F}^{-1}dr^2), \quad (84)$$

where $\hat{F} = -\frac{1}{R}\sqrt{\frac{\chi}{|1+y|}}G$. Since the integral of $\hat{F}^{-1}$ diverges at the event horizon and is finite at $y = -1$ (which corresponds *both* to an axis of rotation and the asymptotic region at infinity), the analysis in Sec. II shows that the corresponding projection diagram is as in Fig. 13.

It is instructive to compare this to the projection diagram for five-dimensional Minkowski space-time

$$(t, \hat{r}\cos\phi, \hat{r}\sin\phi, \tilde{r}\cos\psi, \tilde{r}\sin\psi) \equiv (t, \hat{x}, \hat{y}, \tilde{x}, \tilde{y}) \in \mathbb{R}^5$$

parameterized by ring-type coordinates:

$$y = -\frac{\hat{r}^2}{(\hat{r}^2+\tilde{r}^2)^2} - 1, \qquad x = \frac{\tilde{r}^2}{(\hat{r}^2+\tilde{r}^2)^2} - 1,$$
$$\hat{r} = \sqrt{\hat{x}^2+\hat{y}^2}, \qquad \tilde{r} = \sqrt{\tilde{x}^2+\tilde{y}^2}.$$

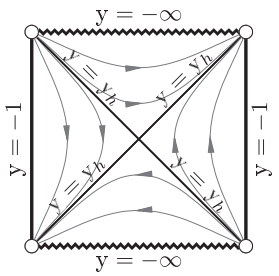

FIG. 13. The projection diagram for the Emparan-Reall black rings. The arrows indicate the causal character of the orbits of the isometry group. The boundary $y = -1$ is covered, via the projection map, by the axis of rotation *and* by spatial infinity i^0. Curves approaching the conformal null infinities $\mathcal{I}^{\pm}$ asymptote to the missing corners in the diagram.

For fixed $x \neq 0$, $y \neq 0$ we obtain a torus as φ and ψ vary over S^1. The image of the resulting map is the set $x \geq -1$, $y \leq -1$, $(x, y) \neq (-1, -1)$. Since

$$x - y = \frac{1}{\hat{r}^2 + \tilde{r}^2},$$

the spheres $\hat{r}^2 + \tilde{r}^2 =: r^2 = \text{const}$ are mapped to subsets of the lines $x = y + 1/r^2$, and the limit $r \to \infty$ corresponds to $0 \leq x - y \to 0$ (hence $x \to -1$ and $y \to -1$). The inverse transformation reads

$$\hat{r} = \frac{\sqrt{-y-1}}{x-y}, \qquad \tilde{r} = \frac{\sqrt{x+1}}{x-y}.$$

The Minkowski metric takes the form

$$\begin{aligned}\eta &= -dt^2 + d\hat{x}^2 + d\hat{y}^2 + d\tilde{x}^2 + d\tilde{y}^2 \\ &= -dt^2 + d\hat{r}^2 + \hat{r}^2 d\varphi^2 + d\tilde{r}^2 + \tilde{r}^2 d\psi^2 \\ &= -dt^2 + \frac{dy^2}{4(-y-1)(x-y)^2} \\ &\quad + \underbrace{\frac{dx^2}{4(x+1)(x-y)^2} + \hat{r}^2 d\varphi^2 + \tilde{r}^2 d\psi^2}_{\geq 0}.\end{aligned}$$

Thus, for any η-causal vector X,

$$\eta(X, X) \geq -(X^t)^2 + \frac{(X^y)^2}{4(-y-1)(x-y)^2}.$$

There is a problem with the right-hand side since, at fixed y, x is allowed to go to infinity, and so there is no positive lower bound on the coefficient of $(X^y)^2$. However, if we restrict attention to the set

$$r = \sqrt{\hat{r}^2 + \tilde{r}^2} \geq R$$

for some $R > 0$, we obtain

$$\eta(X, X) \geq -(X^t)^2 + \frac{R^4 (X^y)^2}{4(-y-1)}.$$

This leads to the conformal projection metric, for $-1 - \frac{1}{R^2} =: y_R \leq y \leq -1$,

$$\begin{aligned}\gamma &:= -dt^2 + \frac{R^4 dy^2}{4|y+1|} = -dt^2 + (d(R^2\sqrt{|y+1|}))^2 \\ &= \frac{R^2}{2\sqrt{|y+1|}} \times \left(-\frac{2\sqrt{|y+1|}}{R^2} dt^2 + \frac{R^2}{2\sqrt{|y+1|}} dy^2 \right).\end{aligned} \tag{85}$$

Introducing a new coordinate $y' = -R^2\sqrt{-y-1}$ we have

$$\gamma = -dt^2 + dy'^2,$$

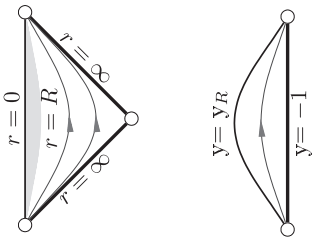

FIG. 14. The projection diagram for the complement of a world-tube $\mathbb{R} \times B(R)$ in five-dimensional Minkowski space-time using spherical coordinates (left figure, where the shaded region has to be removed) or using ring coordinates (right figure). In the right figure the right boundary $y = -1$ is covered, via the projection map, both by the axis of rotation and by spatial infinity, while null infinity projects to the missing points at the top and at the bottom of the diagram.

where $-1 \leq y' \leq 0$. Therefore, the projection diagram corresponds to a subset of the standard diagram for a two-dimensional Minkowski space-time; see Fig. 14.

I. The Pomeransky-Senkov metrics

We consider the *Pomeransky-Senkov metrics* [22]

$$\begin{aligned}g = &\frac{2H(x,y)k^2}{(1-\nu)^2(x-y)^2}\left(\frac{dx^2}{G(x)} - \frac{dy^2}{G(y)}\right) - 2\frac{J(x,y)}{H(y,x)} d\varphi d\psi \\ &- \frac{H(y,x)}{H(x,y)}(dt + \Omega)^2 - \frac{F(x,y)}{H(y,x)} d\psi^2 + \frac{F(y,x)}{H(y,x)} d\varphi^2,\end{aligned} \tag{86}$$

where Ω is a 1-form given by

$$\Omega = M(x, y) d\psi + P(x, y) d\varphi.$$

The definitions of the metric functions may be found in Refs. [22,23]. The metric depends on three constants: k, ν, and λ, where k is assumed to be in $\mathbb{R}^*$, while the parameters λ and ν are restricted to the set [24]

$$\{(\nu, \lambda):\ \nu \in (0, 1),\ 2\sqrt{\nu} \leq \lambda < 1 + \nu\}. \tag{87}$$

The coordinates x, y, φ, ψ, and t vary within the ranges $-1 \leq x \leq 1$, $-\infty < y < -1$, $0 \leq \varphi \leq 2\pi$, $0 \leq \psi \leq 2\pi$ and $-\infty < t < \infty$, respectively.

A Cauchy horizon is located at

$$y_c := -\frac{\lambda + \sqrt{\lambda^2 - 4\nu}}{2\nu},$$

and the event horizon corresponds to

$$y_h := -\frac{\lambda - \sqrt{\lambda^2 - 4\nu}}{2\nu}.$$

Using an appropriate Gauss diagonalization, the metric may be rewritten in the form

$$g = (*) dt^2 + g_{yy} dy^2 + (**),$$

where

$$(*) = (g_{t\psi}^2 g_{\varphi\varphi} - 2g_{t\varphi}g_{t\psi}g_{\psi\varphi} + g_{t\varphi}^2 g_{\psi\psi} + g_{tt}(g_{\psi\varphi}^2 - g_{\varphi\varphi}g_{\psi\psi}))/(g_{\psi\varphi}^2 - g_{\varphi\varphi}g_{\psi\psi}),$$

$$(**) = g_{xx}dx^2 + \frac{(g_{t\psi}dt + g_{\psi\varphi}d\varphi + g_{\psi\psi}d\psi)^2}{g_{\psi\psi}} + \left(g_{\varphi\varphi} - \frac{g_{\psi\varphi}^2}{g_{\psi\psi}}\right)\left(d\varphi + \frac{g_{t\varphi}g_{\psi\psi} - g_{t\psi}g_{\psi\varphi}}{g_{\varphi\varphi}g_{\psi\psi} - g_{\psi\varphi}^2}dt\right)^2.$$

The positive-definiteness of (**) for $y > y_c$ follows from Refs. [21,25]. Note that $g_{\psi\psi} < 0$ would give a timelike Killing vector ∂_ψ and that $g_{\varphi\varphi}g_{\psi\psi} - g_{\psi\varphi}^2 < 0$ would lead to some combination of the periodic Killing vectors ∂_φ and ∂_ψ being timelike, so the term (**) in (88) is non-negative on any region where there are no obvious causality violations.

The coefficient (*) in front of dt^2 is negative for $y > y_h$ and positive for $y < y_h$, vanishing at $y = y_h$. This may be seen in the reparameterized form of the Pomeransky-Senkov solution that was introduced in Ref. [21]: Indeed, let a, b be the new coordinates as in Ref. [21] replacing x and y, respectively, and let us reparameterize ν, λ by c, d again as in Ref. [21], where all the variables a, b, c, d are non-negative above the Cauchy horizon, $y > y_c$:

$$x = -1 + \frac{2}{1+a}, \quad y = -1 - \frac{d(4+c+2d)}{(1+b)(2+c)}, \qquad \nu = \frac{1}{(1+d)^2}, \quad \lambda = 2\frac{2d^2 + 2(2+c)d + (2+c)^2}{(2+c)(1+d)(2+c+2d)}. \tag{88}$$

Set

$$\kappa := (*)\Omega^2, \tag{89}$$

$$\Omega^2 := \frac{(x-y)^2(1-\nu)^2}{2k^2 H(x,y)}. \tag{90}$$

Using MATHEMATICA one finds that κ takes the form

$$\kappa = -\Omega^2(y - y_h)Q,$$

where $Q = Q(a, b, c, d)$ is a huge rational function in (a, b, c, d) with *all coefficients positive*. To obtain the corresponding projection metric γ one would have, e.g., to find sharp lower and upper bounds for Q, at fixed y, which would lead to

$$\gamma := -(y - y_h)\sup_{\text{y fixed}} |Q| dt^2 - \frac{1}{G(y)}dy^2.$$

This requires analyzing a complicated rational function, which we have not been able to do so far. We hope to return to this issue in the future.

We expect the corresponding projection diagram to look like that for Kerr-anti de Sitter space-time of Fig. 12, with $r = \infty$ there replaced by $y = -1$, $r = -\infty$ replaced by $y = 1$ with an appropriate analytic continuation of the metric to positive y's (compare [25]), r_+ replaced by y_h and r_- replaced by y_c. The shaded regions in the negative region there might be nonconnected for some values of parameters and always extend to the boundary at infinity in the relevant diamond [25].

Recall that a substantial part of the work in Ref. [25] was to show that the function $H(x, y)$ had no zeros for $y > y_c$. We note that the reparameterization

$$y \to -1 - \frac{cd}{(1+b)(2+c+2d)}$$

of Ref. [21] [with the remaining formulas (88) remaining the same] gives

$$H(x,y) = \frac{P(a,b,c,d)}{(1+a)^2(1+b)^2(2+c)^2(1+d)^6(2+c+2d)^4},$$

where P is a huge polynomial with *all coefficients positive* for $y > y_h$. This establishes immediately positivity of $H(x, y)$ in the domain of outer communications. We have, however, not been able to find a simple proof of positivity of $H(x, y)$ in the whole range $y > y_c$.

IV. AN APPLICATION TO SPATIALLY COMPACT U(1) × U(1) SYMMETRIC MODELS WITH COMPACT CAUCHY HORIZONS

In this section we wish to use the Kerr-Newman-(anti)de Sitter family of metrics to construct explicit examples of maximal, four-dimensional, U(1) × U(1) symmetric, electrovacuum or vacuum models, with or without cosmological constant, containing a spatially compact partial Cauchy surface. Similarly, five-dimensional, U(1) × U(1) × U(1) symmetric, spatially compact vacuum models with spatially compact partial Cauchy surfaces can be constructed using the Emparan-Reall or Pomeransky-Senkov metrics. We will show how the projection diagrams constructed so far can be used to understand maximal (nonglobally hyperbolic) extensions of the maximal globally hyperbolic regions in such models, and for the Taub-NUT metrics.

A. Kerr-Newman-(anti)de Sitter-type and Pomeransky-Senkov-type models

The diamonds and triangles which have been used to construct our diagrams so far will be referred to as *blocks*. Here the notion of a triangle is understood *up to diffeomorphism*; thus planar sets with three corners, connected by smooth curves intersecting only at the corners which are *not* necessarily straight lines, are also considered to be triangles.

In the interior of each block one can periodically identify points lying along the orbits of the action of the $\mathbb{R}$ factor of the isometry group. Here we are only interested in the connected component of the identity of the group,

which is $\mathbb{R} \times \mathrm{U}(1)$ in the four-dimensional case and $\mathbb{R} \times \mathrm{U}(1) \times \mathrm{U}(1)$ in the five-dimensional case.

Note that isometries of space-time extend smoothly across all block boundaries. For example, in the coordinates $(v, r, \theta, \tilde{\varphi})$ discussed in the paragraph around (30), translations in t become translations in v; similarly for the $(u, r, \theta, \tilde{\varphi})$ coordinates. Using the $(U, V, \theta, \tilde{\varphi})$ local coordinates near the intersection of two Killing horizons, translations in t become boosts in the (U, V) plane.

Consider one of the blocks, out of any of the diagrams constructed above, in which the orbits of the isometry group are spacelike. (Note that no such diamond or triangle has a shaded area which needs to be excised, as the shadings occur only within those building blocks where the isometry orbits are timelike.) It can be seen that the periodic identifications result then in a spatially compact maximal globally hyperbolic space-time with $S^1 \times S^2$ spatial topology, respectively, with $S^1 \times S^1 \times S^2$ topology.

Now, each diamond in our diagrams has four null boundaries which naturally split into pairs, as follows: In each block in which the isometry orbits are spacelike, we will say that two boundaries are *orbit-adjacent* if both boundaries lie to the future of the block or both to the past. In a block where the isometry orbits are timelike, boundaries will be said *orbit-adjacent* if they are both to the left or both to the right.

One out of each pair of orbit-adjacent null boundaries of a block with spacelike isometry-orbits corresponds, in the periodically identified space-time, to a compact Cauchy horizon across which the space-time can be continued to a periodically identified adjacent block. Which of the two adjacent boundaries will become a Cauchy horizon is a matter of choice; once such a choice has been made, the other boundary *cannot* be attached anymore: those geodesics which, in the unidentified space-time, would have been crossing the second boundary become, in the periodically identified space-time, incomplete inextendible geodesics. This behavior is well known from Taub-NUT space-times [26–28] and is easily seen as follows.

Consider a sequence of points $p_i := (t_i, r_i)$ such that p_i converges to a point p on a horizon in a projection diagram in which no periodic identifications have been made. Let $T > 0$ be the period with which the points are identified along the isometry orbits; thus, for every $n \in \mathbb{Z}$ points (t, r) and $(t + nT, r)$ represent the same point of the quotient manifold. It should be clear from the form of the Eddington-Finkelstein-type coordinates u and v used to perform the two distinct extensions [see the paragraph around (30)] that there exists a sequence $n_i \in \mathbb{Z}$ such that, passing to a subsequence if necessary, the sequence $q_i = (t_i + n_i T, r_i)$ converges to some point q in the companion orbit-adjacent boundary; see Fig. 15.

Denote by $[p]$ the class of p under the equivalence relation $(t, r) \sim (t + nT, r)$, where $n \in \mathbb{Z}$ and T is the period. Suppose that one could construct simultaneously

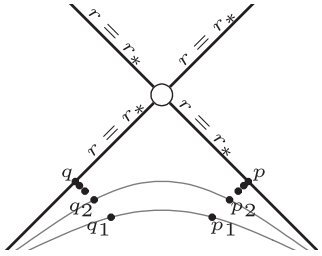

FIG. 15. The sequences q_i and p_i. Rotating the figure by integer multiples of 90° shows that the problem of nonunique limits arises on any pair of orbit-adjacent boundaries.

an extension of the quotient manifold across both orbit-adjacent boundaries. Then the sequence of points $[q_i] = [p_i]$ would have two distinct points $[p]$ and $[q]$ as limit points, which is not possible. This establishes our claim.

Returning to our main line of thought, note that a periodically identified building block in which the isometry orbits are timelike will have obvious causality violations throughout, as a linear combination of the periodic Killing vectors becomes timelike there.

The branching construction, where one out of the pair of orbit-adjacent boundaries is chosen to perform the extension, can be continued at each block in which the isometry orbits are spacelike. This shows that maximal extensions are obtained from any connected union of blocks such that in each block an extension is carried out across precisely one out of each pair of orbit-adjacent boundaries. Some such subsets of the plane might only comprise a finite number of blocks, as seen trivially in Fig. 9. Clearly an infinite number of distinct finite, semi-infinite, or infinite sequences of blocks can be constructed in the diagram of Fig. 6. Two sequences of blocks which are not related by one of the discrete isometries of the diagram will lead to nonisometric maximal extensions of the maximal globally hyperbolic initial region.

B. Taub-NUT metrics

We have seen at the end of Sec. III B how to construct a projection diagram for Gowdy cosmological models. Those models all contain $\mathrm{U}(1) \times \mathrm{U}(1)$ as part of their isometry group. The corresponding projection diagrams constructed in Sec. III B were obtained by projecting out the isometry orbits. This is rather different from the remaining projection diagrams constructed in this work, where only one of the coordinates along the Killing orbits was projected out.

It is instructive to carry out explicitly both procedures for the Taub-NUT metrics, which belong to the Gowdy class. Using Euler angles (ζ, θ, φ) to parameterize S^3, the Taub-NUT metrics [26,29] take the form

$$g = -U^{-1} dt^2 + (2\ell)^2 U (d\zeta + \cos(\theta) d\varphi)^2 + (t^2 + \ell^2)(d\theta^2 + \sin^2(\theta) d\varphi^2). \tag{91}$$

Here

$$U(t) = -1 + \frac{2(mt + \ell^2)}{t^2 + \ell^2} = \frac{(t_+ - t)(t - t_-)}{t^2 + \ell^2},$$

with

$$t_\pm := m \pm \sqrt{m^2 + \ell^2}.$$

Further, ℓ and m are real numbers with $\ell > 0$. The region $\{t \in (t_-, t_+)\}$ will be referred to as the *Taub space-time*.

The metric induced on the sections $\theta = \text{const}$, $\varphi = \text{const}'$, of the Taub space-time reads

$$\gamma_0 := -U^{-1}dt^2 + (2\ell)^2 U d\zeta^2. \tag{92}$$

As already discussed by Hawking and Ellis [1], this is a metric to which the methods of Sec. II apply *provided that the 4π-periodic identifications in ζ are relaxed*. Since U has two simple zeros, and no singularities, the conformal diagram for the corresponding maximally extended two-dimensional space-time equipped with the metric γ_0 can be seen as the left diagram in Fig. 16; compare Fig. 33 in Ref. [1]. The discussion of the last paragraph of the previous section applies and, together with the left diagram in Fig. 16, provides a family of simply connected maximal extensions of the sections $\theta = \text{const}$, $\varphi = \text{const}'$, of the Taub space-time.

However, it is not clear how to relate the above to extensions of the four-dimensional space-time. Note that

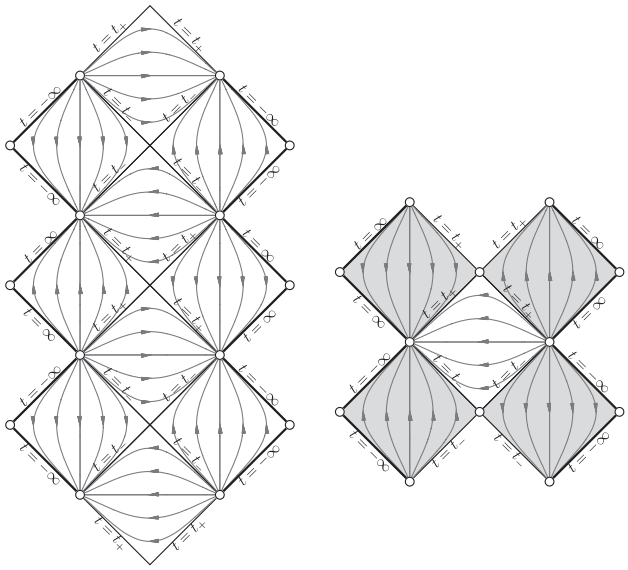

FIG. 16. The left diagram is the conformal diagram for an extension of the universal covering space of the sections $\theta = \text{const}$, $\varphi = \text{const}'$, of the Taub space-time. The right diagram represents simultaneously the four possible diagrams for the maximal extensions, within the Taub-NUT class, with compact Cauchy horizons, of the Taub space-time. After invoking the left-right symmetry of the diagram, which lifts to an isometry of the extended space-time, the four diagrams lead to two non-isometric space-times.

projecting out the ζ and φ variables in the region where $U > 0$, using the projection map $\pi_1(t, \zeta, \theta, \varphi) := (t, \theta)$, one is left with the two-dimensional metric

$$\gamma_1 := -U^{-1}dt^2 + (t^2 + \ell^2)d\theta^2, \tag{93}$$

which leads to the flat metric on the Gowdy square as the projection metric. (The coordinate t here is not the same as the Gowdy t coordinate, but the projection diagram remains a square.) And one is left wondering how this fits with the previous picture.

Now, one can attempt instead to project out the θ and φ variables, with the projection map

$$\pi_2(t, \zeta, \theta, \varphi) := (t, \zeta). \tag{94}$$

For this we note the trivial identity

$$\begin{aligned} &g_{\zeta\zeta}d\zeta^2 + 2g_{\varphi\zeta}d\varphi d\zeta + g_{\varphi\varphi}d\varphi^2 \\ &\quad = \left(g_{\zeta\zeta} - \frac{g_{\varphi\zeta}^2}{g_{\varphi\varphi}}\right)d\zeta^2 + \underbrace{g_{\varphi\varphi}\left(d\varphi + \frac{g_{\varphi\zeta}}{g_{\varphi\varphi}}d\zeta\right)^2}_{(*)}. \end{aligned} \tag{95}$$

Since the left-hand side is positive-definite on Taub space, where $U > 0$, both $g_{\zeta\zeta} - \frac{g_{\varphi\zeta}^2}{g_{\varphi\varphi}}$ and $g_{\varphi\varphi}$ are non-negative there. Indeed,

$$g_{\varphi\varphi} = (\ell^2 + t^2)\sin^2(\theta) + 4\ell^2 U\cos^2(\theta), \tag{96}$$

$$\begin{aligned} g_{\zeta\zeta} - \frac{g_{\varphi\zeta}^2}{g_{\varphi\varphi}} &= (2\ell)^2\left(1 - \frac{(2\ell)^2 U\cos^2(\theta)}{g_{\varphi\varphi}}\right)U \\ &= \underbrace{\frac{4\ell^2(\ell^2 + t^2)\sin^2(\theta)}{(\ell^2 + t^2)\sin^2(\theta) + 4\ell^2 U\cos^2(\theta)}}_{(**)}U. \end{aligned} \tag{97}$$

However, perhaps not unsurprisingly given the character of the coordinates involved, the function $(**)$ in (97) does not have a positive lower bound independent of $\theta \in [0, 2\pi]$, which is unfortunate for our purposes. To sidestep this drawback we choose a number $0 < \epsilon < 1$ and restrict ourselves to the range $\theta \in [\theta_\epsilon, \pi - \theta_\epsilon]$, where $\theta_\epsilon \in [0, \pi/2]$ is defined by

$$\sin^2(\theta_\epsilon) = \epsilon.$$

Now, $g_{\varphi\varphi}$ is positive for large t, independently of θ. Next, $g_{\varphi\varphi}$ equals $4\ell^2 U$ at the axes of rotation $\sin(\theta) = 0$ and equals $\ell^2 + t^2$ at $\theta = \pi/2$. Hence, keeping in mind that U is monotonic away from (t_-, t_+), for ϵ small enough there will exist values

$$\hat{t}_\pm(\epsilon), \quad \text{with} \quad \hat{t}_-(\epsilon) < t_- < 0 < t_+ < \hat{t}_+(\epsilon)$$

such that $g_{\varphi\varphi}$ will be negative somewhere in the region $(\hat{t}_-(\epsilon), t_-) \cup (t_+, \hat{t}_+(\epsilon))$ and will be positive outside of this

region. We choose those numbers to be optimal with respect to those properties.

On the other hand, for ϵ close enough to 1 the metric coefficient $g_{\varphi\varphi}$ will be positive for all $\theta \in [\theta_\epsilon, \pi - \theta_\epsilon]$ and $t < t_-$. In this case we set $\hat{t}_-(\epsilon) = t_-$, so that the interval $(\hat{t}_-(\epsilon), t_-)$ is empty. Similarly, there will exist a range of ϵ for which $\hat{t}_+(\epsilon) = t_+$, and $(t_+, \hat{t}_+(\epsilon)) = \varnothing$. The relevant ranges of ϵ will coincide only if $m = 0$.

We note

$$\partial_\theta\left(g_{\zeta\zeta} - \frac{g_{\varphi\zeta}^2}{g_{\varphi\varphi}}\right) = \frac{16\ell^4 U^2(\ell^2 + t^2)\sin(2\theta)}{((\ell^2 + t^2)\sin^2(\theta) + 4\ell^2 U\cos^2(\theta))^2},$$

which shows that, for

$$t \notin (\hat{t}_-(\epsilon), t_-) \cup (t_+, \hat{t}_+(\epsilon)) \quad \text{and} \quad \theta \in (\theta_\epsilon, \pi - \theta_\epsilon), \quad (98)$$

the multiplicative coefficient $(**)$ of U in (97) will satisfy

$$(**) \geq \frac{4\ell^2(\ell^2 + t^2)\sin^2(\theta_\epsilon)}{(\ell^2 + t^2)\sin^2(\theta_\epsilon) + 4\ell^2 U\cos^2(\theta_\epsilon)} =: f_\epsilon(t). \quad (99)$$

We are ready now to construct the projection metric in the region (98). Removing from the metric tensor (91) the terms $(*)$ appearing in (95), as well as the $d\theta^2$ terms, and using (99) one finds, for g-causal vectors X,

$$g(X, X) \geq \gamma_2((\pi_2)_* X, (\pi_2)_* X),$$

with π_2 as in (94), where

$$\gamma_2 := -U^{-1}dt^2 + f_\epsilon U d\zeta^2. \quad (100)$$

Since U has exactly two simple zeros and is finite everywhere, and for ϵ such that $g_{\varphi\varphi}$ is positive on the region $\theta \in [\theta_\epsilon, \pi - \theta_\epsilon]$, the projection diagram for that region, *in a space-time in which no periodic identifications in ζ are made*, is given by the left diagram of Fig. 16. The reader should have no difficulties finding the corresponding diagrams for the remaining values of ϵ.

However, we are in fact interested in those space-times where ζ is 4π periodic. This has two consequences: (i) there are closed timelike Killing orbits in all the regions where U is negative, and (ii) no simultaneous extensions are possible across two orbit-adjacent boundaries. It then follows (see the right diagram of Fig. 16) that there are, within the Taub-NUT class, only two nonisometric, maximal, vacuum extensions across compact Cauchy horizons of the Taub space-time. (Compare Proposition 4.5 and Theorem 1.2 in Ref. [30] for the local uniqueness of extensions and [31] for a discussion of extensions with noncompact Killing horizons.)

ACKNOWLEDGMENTS

P. T. C. was supported in part by Narodowe Centrum Nauki under Grant No. DEC-2011/03/B/ST/02625. S. J. S. was supported by the John Templeton Foundation and would like to thank the University of Vienna for hospitality.

[1] S. Hawking and G. Ellis, *The Large Scale Structure of Space-Time*, Cambridge Monographs on Mathematical Physics Vol. 1 (Cambridge University Press, Cambridge, England, 1973).
[2] B. Carter, Phys. Rev. **174**, 1559 (1968).
[3] B. Carter, in *Black Holes, Proceedings of the Les Houches Summer School*, edited by C. de Witt and B. de Witt (Gordon and Breach, New York, 1973).
[4] G. Gibbons and S. Hawking, Phys. Rev. D **15**, 2738 (1977).
[5] M. Walker, J. Math. Phys. (N.Y.) **11**, 2280 (1970).
[6] R. Gowdy, Phys. Rev. Lett. **27**, 826 (1971).
[7] P. Chruściel, Ann. Phys. (N.Y.) **202**, 100 (1990).
[8] H. Ringström, Classical Quantum Gravity **22**, 1647 (2005).
[9] H. Ringström, Ann. Math. **170**, 1181 (2009).
[10] Once this work was written it was pointed out to us that the idea of using the Penrose diagram for the quotient-space metric has been used in Ref. [11]. The Penrose-Carter conformal diagram of Sec. 4.6 of Ref. [11] coincides with a projection diagram for the Breckenridge-Myers-Peet-Vafa metric, but our interpretation of this diagram differs.
[11] G. Gibbons and C. Herdeiro, Classical Quantum Gravity **16**, 3619 (1999).
[12] M. Demiański, Acta Astronomica **23**, 197 (1973).
[13] B. Carter, Commun. Math. Phys. **10**, 280 (1968).
[14] S. Akcay and R. Matzner, Classical Quantum Gravity **28**, 085012 (2011).
[15] H. Stephani, D. Kramer, M. MacCallum, C. Hoenselaers, and E. Herlt, *Exact Solutions of Einstein's Field Equations*, Cambridge Monographs on Mathematical Physics (Cambridge University Press, Cambridge, England, 2003), 2nd ed.
[16] The transition from the formulas in Ref. [13] to (43) is explained in Ref. [3], p. 102.
[17] We, and Kayll Lake (private communication), calculated several curvature invariants for the overspinning metrics and found no singularity at $\Delta_\theta = 0$. The origin of this surprising fact is not clear to us.
[18] M. Henneaux and C. Teitelboim, Commun. Math. Phys. **98**, 391 (1985).

[19] R. Emparan and H. Reall, Living Rev. Relativity **11**, 6 (2008).
[20] R. Emparan and H. Reall, Phys. Rev. Lett. **88**, 101101 (2002).
[21] P. Chruściel and S. Szybka, Adv. Theor. Math. Phys. **15**, 175 (2011).
[22] A. Pomeransky and R. Senkov, arXiv:hep-th/0612005.
[23] We use (ψ, φ) where Pomeransky and Senkov use (φ, ψ).
[24] $\nu = 0$ corresponds to the Emparan-Reall metric which has been already analyzed in Sec. III H.
[25] P. Chruściel, J. Cortier, and A. Garcia-Parrado, Adv. Theor. Math. Phys. **14**, 1779 (2010).
[26] A. Taub, Ann. Math. **53**, 472 (1951).
[27] P. Chruściel and J. Isenberg, Phys. Rev. D **48**, 1616 (1993).
[28] C. Misner, in *Relativity Theory and Astrophysics*, Lect. Appl. Math. Vol. 8 (American Mathematical Society, Providence, 1967), p. 160–169.
[29] E. Newman, L. Tamburino, and T. Unti, J. Math. Phys. (N.Y.) **4**, 915 (1963).
[30] P. Chruściel and A. Rendall, Ann. Phys. (N.Y.) **242**, 349 (1995).
[31] P. Chruściel, J. Diff. Geom. **84**, 19 (2010).